Stabilizing negative charge in organic molecules for high-efficiency, long-lifetime delayed electroluminescence

Tianyu Huang[1], Qi Wang[1], Yangyang Xin[1], Hai Zhang[1], Guomeng Li[1], Yuewei Zhang[1], Dongdong Zhang[1]*, Lian Duan[1,3]*

[1] Key Laboratory of Organic Optoelectronics, Department of Chemistry, Tsinghua University, Beijing 100084, China

[2] Laboratory of Flexible Electronics Technology， Tsinghua University, Beijing 100084, China.

E-mail: ddzhang@mail.tsinghua.edu.cn; duanl@mail.tsinghua.edu.cn

Contents

S1. Materials synthesis and characterization

Synthesis of 4CzBN-PhCN. 4CzBN-PhCN was synthesized through a two-step process from 4-bromo-2,3,5,6-tetrafluorobenzonitrile and (4-cyanophenyl)boronic acid. The stepwise synthetic methods are shown in Scheme S1 and the general process is given below.

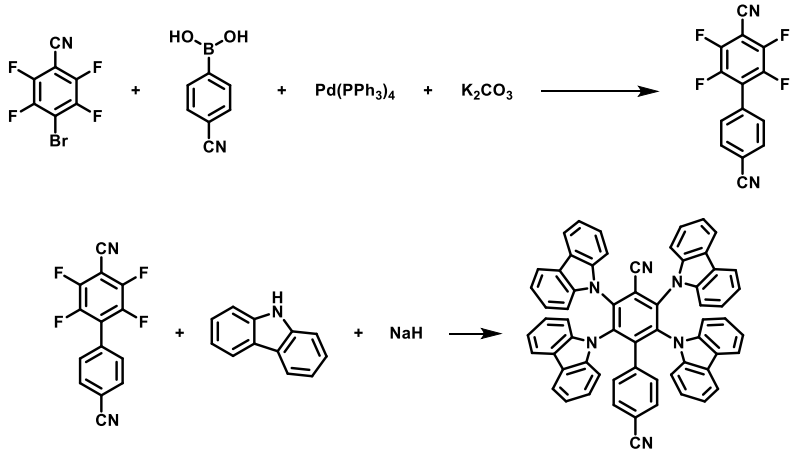

Scheme S1 Synthesis of 4CzBN-PhCN

Synthesis of 2,3,5,6-tetrafluoro-[1,1'-biphenyl]-4,4'-dicarbonitrile. A mixture of 4-bromo-2,3,5,6-tetrafluorobenzonitrile (5.00 g, 19.69 mmol), (4-cyanophenyl)boronic acid (3.18 g, 21.66 mmol), $Pd(PPh_3)_4$ (1.14 g, 0.98 mmol), and potassium carbonate (5.44 g, 39.37 mmol) dissolved in 1,4-dioxane/H_2O in a 2-neck round bottle was refluxed for 12 hours under nitrogen. The water was separated, and the organic layer was extracted with chloroform. The combined organic extracts were dried over Na_2SO_4 and concentrated by rotary evaporation. The crude product was purified by column chromatography on silica gel using 1: 4 dichloromethane (DCM)/petroleum ether (PE) as eluent to afford a white solid (3.90 g, 72 % yield).

Synthesis of 4CzBN-PhCN. A mixture of carbazole (2.66 g, 15.93 mmol) and sodium hydride (60% in mineral oil, 0.87 g, 21.7 mmol) dissolved in dimethyl formaldehyde (DMF) was heated at 80℃ for 1 hour. Then, 2,3,5,6-tetrafluoro-[1,1'-biphenyl]-4,4'-dicarbonitrile (1.00 g, 3.62 mmol) was added to the reaction drop by drop and heated overnight. After cooling to room temperature, the solution was poured into ice water and the precipitation was filtered to get crude product. Afterwards, the product was purified by column chromatography on silica-gel (DCM: PE =5:1) to afford a yellow solid (2.50 g, 2.89 mmol, 80% yield).

^{1}H NMR (400 MHz, Chloroform-*d*) δ 7.76 – 7.69 (m, 4H), 7.61 – 7.54 (m, 4H), 7.24 – 7.20 (m, 4H), 7.12 – 7.06 (m, 8H), 6.95 (m, 12H), 6.73 – 6.62 (dd, J = 11.5, 8.3 Hz, 4H).

^{13}C NMR (101 MHz, Chloroform-*d*) δ 139.3205, 138.9204, 131.2069, 128.1709, 125.5164, 125.2434, 124.1485, 123.3811, 121.2103, 120.7072, 120.2952, 120.1272, 112.2783, 110.0613, 109.6195.

MALDI-TOF-MS m/z: 864.37 [M]+

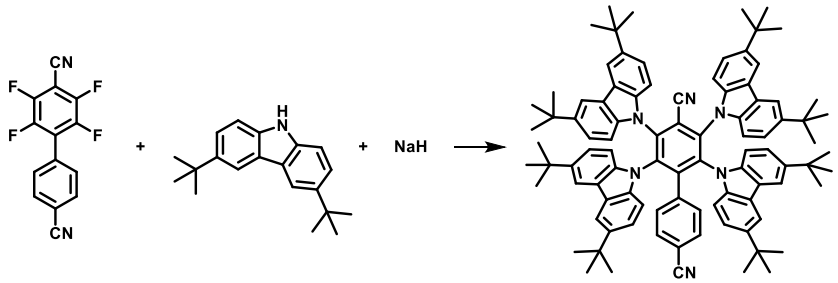

Scheme S2 Synthesis of 4tCzBN-PhCN

Synthesis of 4tCzBN-PhCN. As shown in Scheme S2, a mixture of 3,6-tert-butylcarbazole (4.45 g, 15.93 mmol) and sodium hydride (60% in mineral oil, 0.87 g, 21.7 mmol) dissolved in dimethyl formaldehyde (DMF) was heated at 80℃ for 1 hour. Then, 2,3,5,6-tetrafluoro-[1,1'-biphenyl]-4,4'-dicarbonitrile (1.00 g, 3.62 mmol) was added to the reaction drop by drop and heated overnight. After cooling to room temperature, the solution was poured into ice water and the precipitation was filtered to get crude product. Afterwards, the product was purified by column chromatography on silica-gel (DCM: PE =5:1) to afford a yellow solid (3.96 g, 3.01 mmol, 83% yield).

^{1}H NMR (400 MHz, Chloroform-*d*) δ 7.56 (d, *J* = 1.8 Hz, 4H), 7.45 (d, *J* = 1.8 Hz, 4H), 7.02 (d, *J* = 8.2 Hz, 2H), 6.95 (dd, *J* = 8.7, 1.8 Hz, 4H), 6.87 (d, *J* = 8.5 Hz, 4H), 6.83 (dt, *J* = 8.6, 2.1 Hz, 6H), 6.59 (d, *J* = 8.6 Hz, 4H), 1.34 (s, 36H), 1.30 (s, 36H).

^{13}C NMR (101 MHz, Chloroform-*d*) δ 148.2400, 143.8188, 143.3146, 141.3521, 138.2856, 137.8515, 137.1944, 135.4780, 131.5297, 129.1458, 124.5381, 123.7244, 122.8810, 122.6045, 115.7702, 115.6259, 111.8658, 109.7246, 108.9686, 77.4102, 77.0917, 76.7764, 34.6014, 34.5275, 31.9593, 31.9105.

MALDI-TOF-MS m/z: 1313.47 [M]+

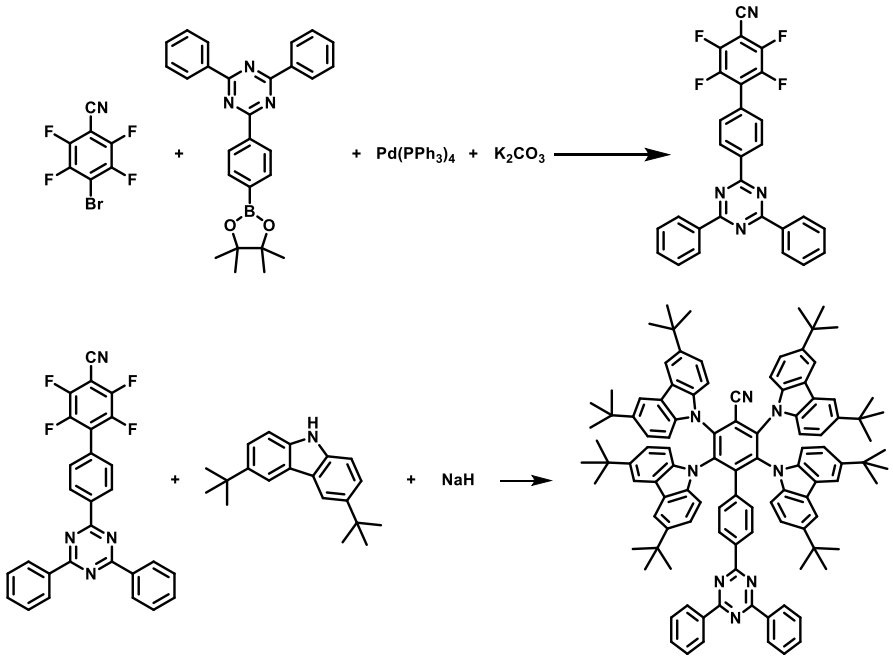

Scheme S3 Synthesis of 4tCzBN-TRZ

Synthesis of 4'-(4,6-diphenyl-1,3,5-triazin-2-yl)-2,3,5,6-tetrafluoro-[1,1'-biphenyl]-4-carbonitrile. A mixture of 4-bromo-2,3,5,6-tetrafluorobenzonitrile (5.00 g, 19.69 mmol), 2,4-

diphenyl-6-(4-(4,4,5,5-tetramethyl-1,3,2-dioxaborolan-2-yl)phenyl)-1,3,5-triazine (9.43 g, 21.66 mmol), $Pd(PPh_3)_4$ (1.14 g, 0.98 mmol), and potassium carbonate (5.44 g, 39.37 mmol) dissolved in 1,4-dioxane/H_2O in a 2-neck round bottle was refluxed for 12 hours under nitrogen. The water was separated, and residue was filtered and washed by DCM. The crude product is a white solid and used directly without further purification due to the poor solubility (5.50 g, 58 % yield).

Synthesis of 4tCzBN-TRZ. A mixture of 3,6-tert-butylcarbazole (2.55 g, 9.12 mmol) and sodium hydride (60% in mineral oil, 0.50 g, 12.44 mmol) dissolved in dimethyl formaldehyde (DMF) was heated at 80℃ for 1 hour. Then, 4'-(4,6-diphenyl-1,3,5-triazin-2-yl)-2,3,5,6-tetrafluoro-[1,1'-biphenyl]-4-carbonitrile (1 g, 2.07 mmol) was added to the reaction drop by drop and heated overnight. After cooling to room temperature, the solution was poured into ice water and the precipitation was filtered to get crude product. Afterwards, the product was purified by column chromatography on silica-gel (DCM: PE =5:1) to afford a yellow solid (2.70 g, 1.78 mmol, 86% yield).

^{1}H NMR (400 MHz, Chloroform-*d*) δ 8.42 (dd, *J* = 7.1, 1.7 Hz, 4H), 8.07 – 7.97 (m, 2H), 7.57 (d, *J* = 1.9 Hz, 4H), 7.43 (q, *J* = 2.8 Hz, 6H), 7.36 (dd, *J* = 8.3, 6.8 Hz, 4H), 6.99 – 6.92 (m, 4H), 6.90 – 6.82 (m, 8H), 6.72 (d, *J* = 8.6 Hz, 4H), 1.36 (s, 36H), 1.28 (s, 36H).

^{13}C NMR (101 MHz, Chloroform-*d*) δ 171.2924, 170.3967, 149.9348, 143.5338, 142.9249, 140.9966, 137.9551, 137.8878, 137.5745, 136.0042, 135.9179, 135.5608, 132.4428, 128.8857, 128.8067, 128.5086, 128.4539, 124.4151, 123.9086, 122.7961, 122.5552, 118.0665, 115.6843, 115.5563, 113.3240, 109.6899, 109.2051, 77.4071, 77.0909, 76.7744, 34.5991, 34.4956, 31.9996, 31.9352.

MALDI-TOF-MS m/z: 1520.02 [M]+

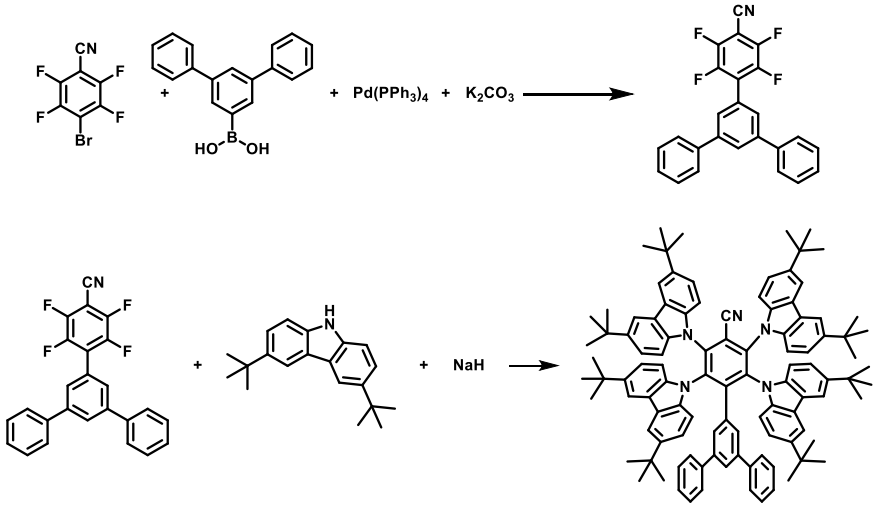

Scheme S4 Synthesis of 4tCzBN-TPh

Synthesis of 2,3,5,6-tetrafluoro-5'-phenyl-[1,1':3',1''-terphenyl]-4-carbonitrile. A mixture of 4-bromo-2,3,5,6-tetrafluorobenzonitrile (5.00 g, 19.69 mmol), [1,1':3',1"-terphenyl]-5'-ylboronic acid (5.94 g, 21.66 mmol), $Pd(PPh_3)_4$ (1.14 g, 0.98 mmol), and potassium carbonate (5.44 g, 39.37 mmol) dissolved in toluene/H_2O in a 2-neck round bottle was refluxed for 12 hours under nitrogen. The water was separated, and the organic layer was extracted with chloroform. The combined organic extracts were dried over Na_2SO_4 and concentrated by rotary evaporation. The crude product was purified by column chromatography on silica gel using 1: 5 dichloromethane (DCM)/petroleum

ether (PE) as eluent to afford a white solid (6.50 g, 82 % yield).

Synthesis of 4tCzBN-TPh. A mixture of 3,6-tert-butylcarbazole (3.05 g, 10.91 mmol) and sodium hydride (60% in mineral oil, 0.59 g, 14.87 mmol) dissolved in dimethyl formaldehyde (DMF) was heated at 80℃ for 1 hour. Then, 2,3,5,6-tetrafluoro-5'-phenyl-[1,1':3',1"-terphenyl]-4-carbonitrile (1 g, 2.48 mmol) was added to the reaction drop by drop and heated overnight. After cooling to room temperature, the solution was poured into ice water and the precipitation was filtered to get crude product. Afterwards, the product was purified by column chromatography on silica-gel (DCM: PE =5:1) to afford a yellow solid (2.90 g, 2.01 mmol, 81% yield).

^{1}H NMR (400 MHz, Chloroform-*d*) δ 7.61 (d, *J* = 1.4 Hz, 4H), 7.49 (d, *J* = 1.8 Hz, 4H), 7.09 – 7.00 (m, 10H), 6.97 – 6.86 (m, 10H), 6.82 (s, 1H), 6.74 (d, *J* = 8.6 Hz, 4H), 6.26 (d, *J* = 7.2 Hz, 4H), 1.35 (s, 36H), 1.29 (s, 36H).

^{13}C NMR (101 MHz, Chloroform-*d*) δ 151.4508, 143.6963, 142.7815, 142.1894, 140.7954, 140.5217, 138.5363, 137.8126, 136.1550, 133.6745, 128.2674, 126.9336, 126.1814, 126.0482, 124.6344, 123.4939, 122.9763, 122.6698, 117.5142, 115.7861, 115.3572, 113.3701, 109.9428, 109.4310, 77.4137, 77.0935, 76.7767, 34.6096, 34.5238, 31.9747.

MALDI-TOF-MS m/z: 1441.00 [M]+

Synthesis of 3Cz2DPhCzBN and 5Cz-TRZ. 3Cz2DPhCzBN and 5Cz-TRZ was synthesized according to the methods reported in the corresponding literature and characterized by NMR and MALDI-TOF-MS.

S2. Quantum chemistry calculation

Supplementary Table 1 Bond dissociation energy values of the TADF emitters

	BDE(-) / eV	BDE / eV	BDE(+) / eV
4CzBN-PhCN	3.78	4.15	4.89
4tCzBN-PhCN	3.94	4.36	5.08
4tCzBN-TRZ	3.84	4.24	4.93
4tCzBN-TPh	3.62	4.36	5.03
3Cz2DPhCzBN	3.47	4.09	4.67
5Cz-TRZ	3.63	4.29	4.73

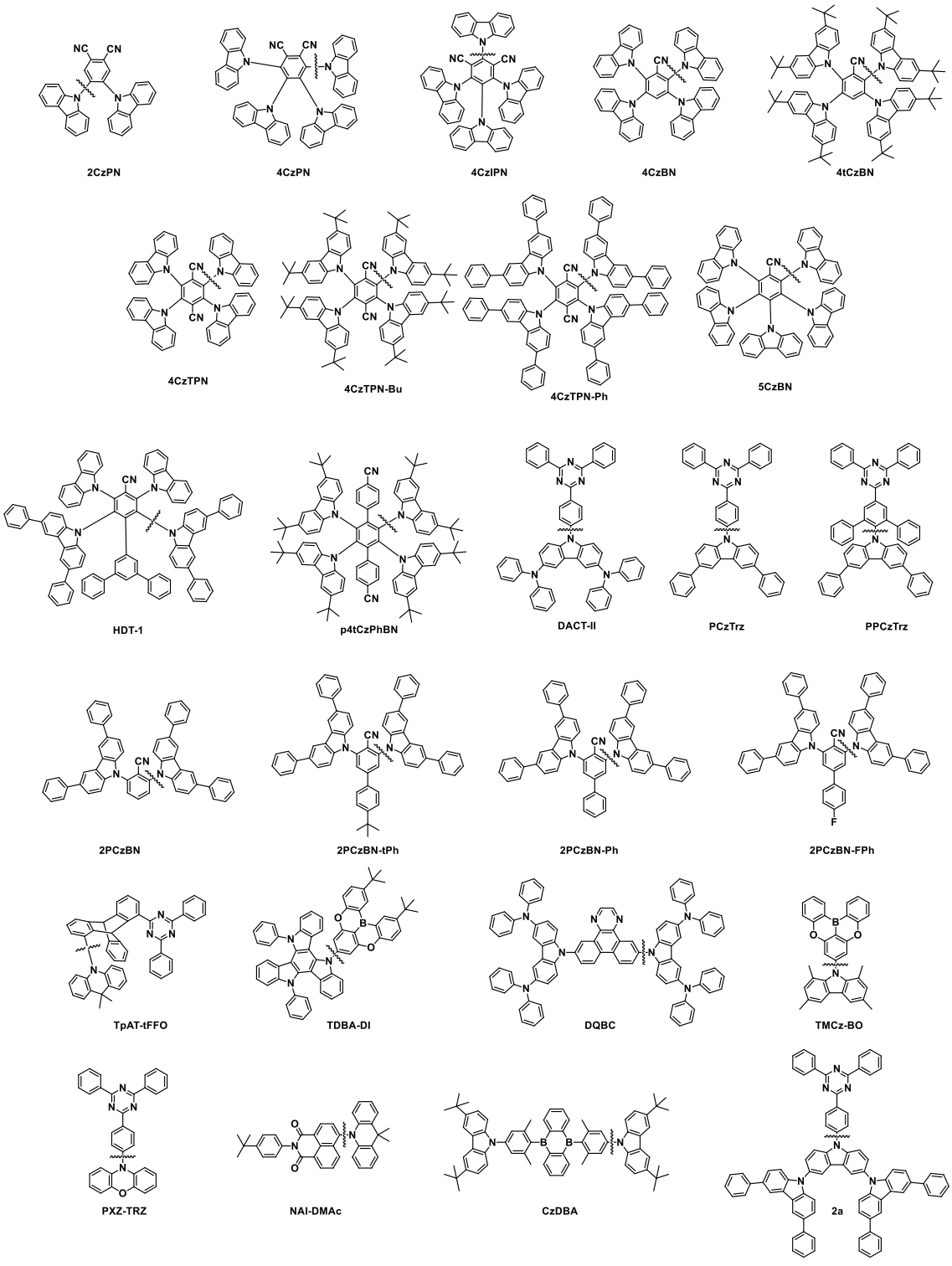

Supplementary Figure 1 Chemical structures of the reported TADF emitters for cross-comparison of BDE values. The positions of the C-N bonds are marked by wavy line in each structure.

Supplementary Table 2 BDE values of the reported TADF emitters for cross-comparison

	BDE(-) / eV	BDE / eV	BDE(+) / eV	Ref.
2CzPN	3.46	3.95	4.09	[5]
4CzPN	3.79	5.06	4.11	[6]
4CzIPN	3.83	4.45	4.21	[6]
4CzBN	3.22	4.53	4.13	[7]
4tCzBN	3.46	5.16	4.41	[7]
4CzTPN	3.98	4.91	4.18	[6]
4CzTPN-Bu	4.15	5.05	4.41	[6]
4CzTPN-Ph	4.21	5.07	4.45	[6]
5CzBN	3.36	4.62	4.08	[7]
HDT-1	3.45	4.96	4.40	[8]
p4tCzPhBN	3.83	5.10	4.36	[9]
DACT-II	2.50	5.88	3.63	[10]
PCzTrz	2.58	5.28	3.83	[11]
PPCzTRZ	2.74	4.97	3.90	[11]
2PCzBN	2.35	4.80	3.80	[12]
2PCzBN-Ph	2.70	4.77	3.82	[12]
2PCzBN-tPh	2.68	4.64	3.82	[12]
2PCzBN-FPh	2.74	4.78	3.82	[12]
TpAT-tFFO	3.50	3.72	4.09	[13]
TDBA-DI	2.12	5.09	3.61	[14]
DQBC	2.52	5.01	3.64	[15]
TMCz-BO	2.48	4.66	3.51	[16]
PXZ-TRZ	2.75	6.83	5.11	[17]
NAI-DMAc	3.35	4.93	3.37	[18]
CzDBA	3.57	4.83	3.84	[19]
2a	2.29	5.73	3.82	[20]

Supplementary Table 3 Spin-orbital coupling constants for the TADF emitters

	S_1 [eV]	T_1	T_2	T_3	ΔE_{S1-T1}	ΔE_{S1-T2}	ΔE_{S1-T3}	λ_{SOC} (S_1-T_1) [cm^{-1}]	λ_{SOC} (S_1-T_2)	λ_{SOC} (S_1-T_3)
4CzBN -PhCN	2.6438	2.5347	2.5877	2.6565	0.1091	0.0561	-0.0127	0.01	0.73	0.20
4tCzBN -PhCN	2.5514	2.4643	2.4893	2.5598	0.0871	0.0621	-0.0084	0.08	0.71	0.21
4tCzBN -TRZ	2.5751	2.4986	2.5158	2.5616	0.0765	0.0593	0.0135	0.05	0.66	0.28
4tCzBN -TPh	2.6761	2.587	2.6247	2.7014	0.0891	0.0514	-0.0253	0.36	0.60	0.40

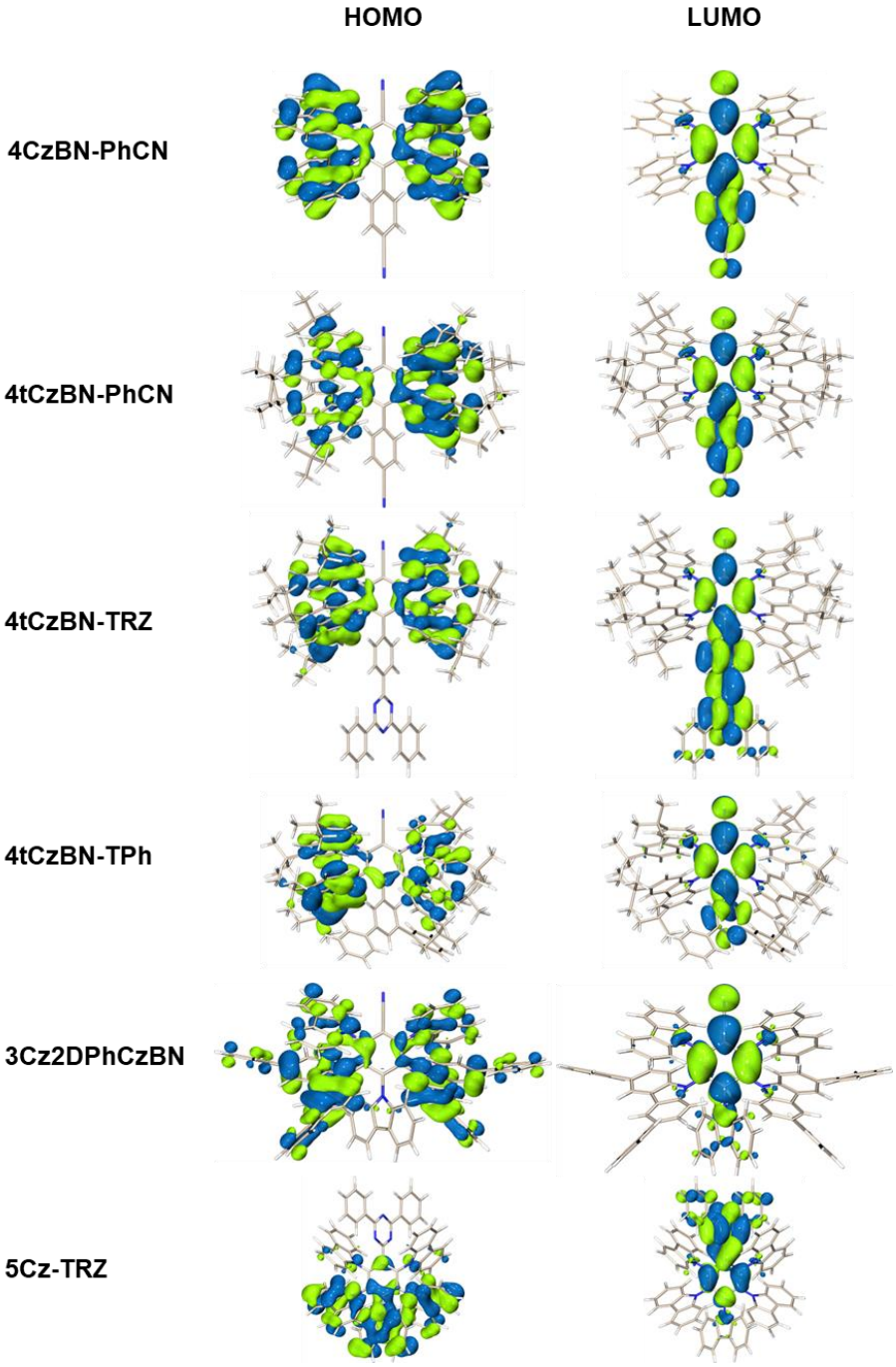

Supplementary Figure 2 HOMO and LUMO distribution of the TADF molecules.

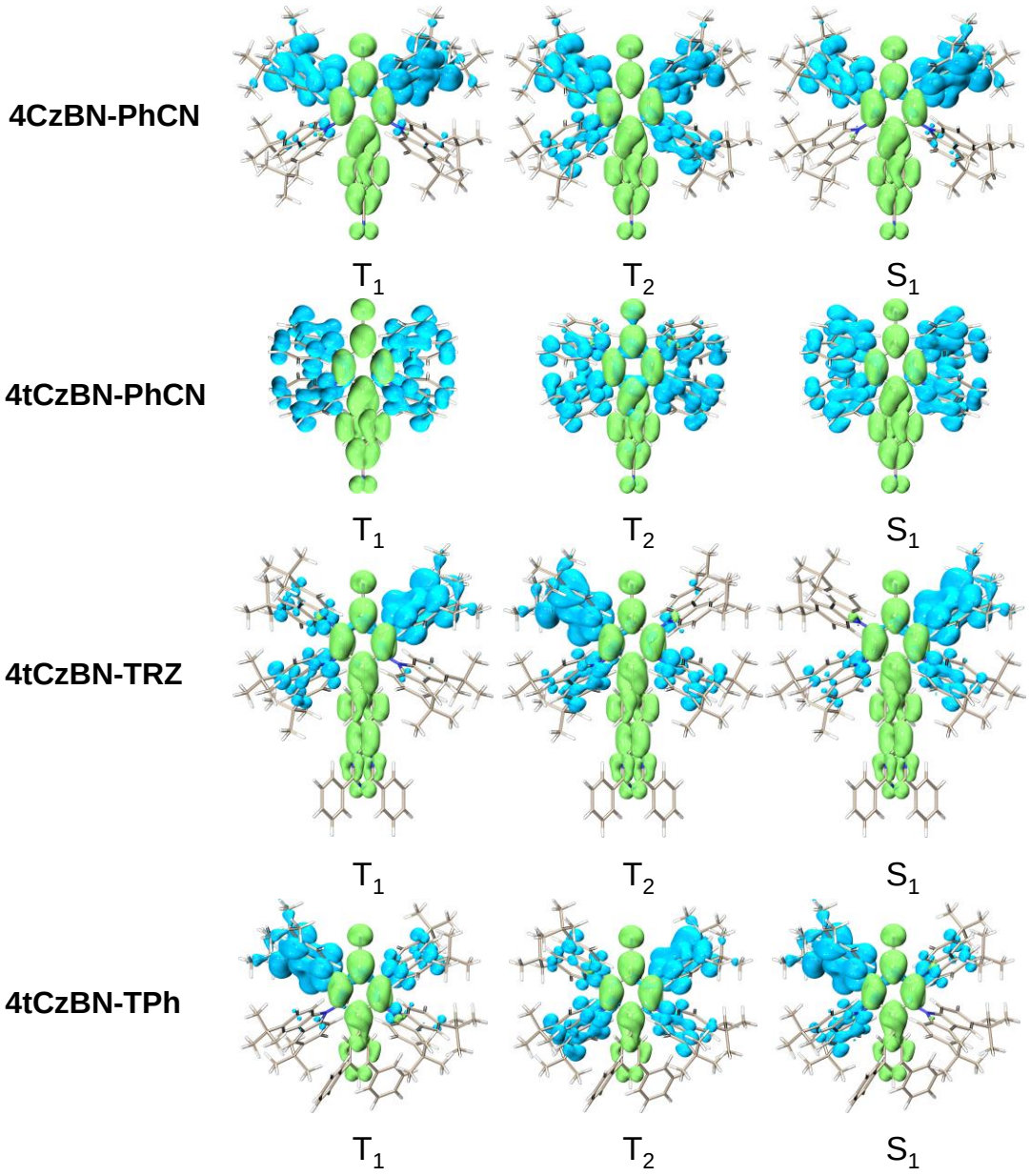

Supplementary Figure 3 Hole-electron analysis of the TADF molecules (Blue isovalue surface for hole distribution and green isovalue surface for electron distribution).

S3. Electrochemical properties

The electrochemical measurements were performed with a Potentiostat/Galvanostat Model 283 (Princeton Applied Research) electrochemical workstation by using Pt as the working electrode, platinum wire as the auxiliary electrode, and an Ag wire as the reference electrode standardized against ferrocene/ferrocenium. The oxidation potentials were measured in dichloromethane (CH_2Cl_2) solution containing 0.1 M n-Bu_4NPF_6 as the supporting electrolyte at a scan rate of 100 mV s^{-1}. The reduction potentials were measured in N, N-Dimethylformamide (DMF) solution containing 0.1 M n-Bu_4NClO_4 as the supporting electrolyte at a scan rate of 100 mV s^{-1}.

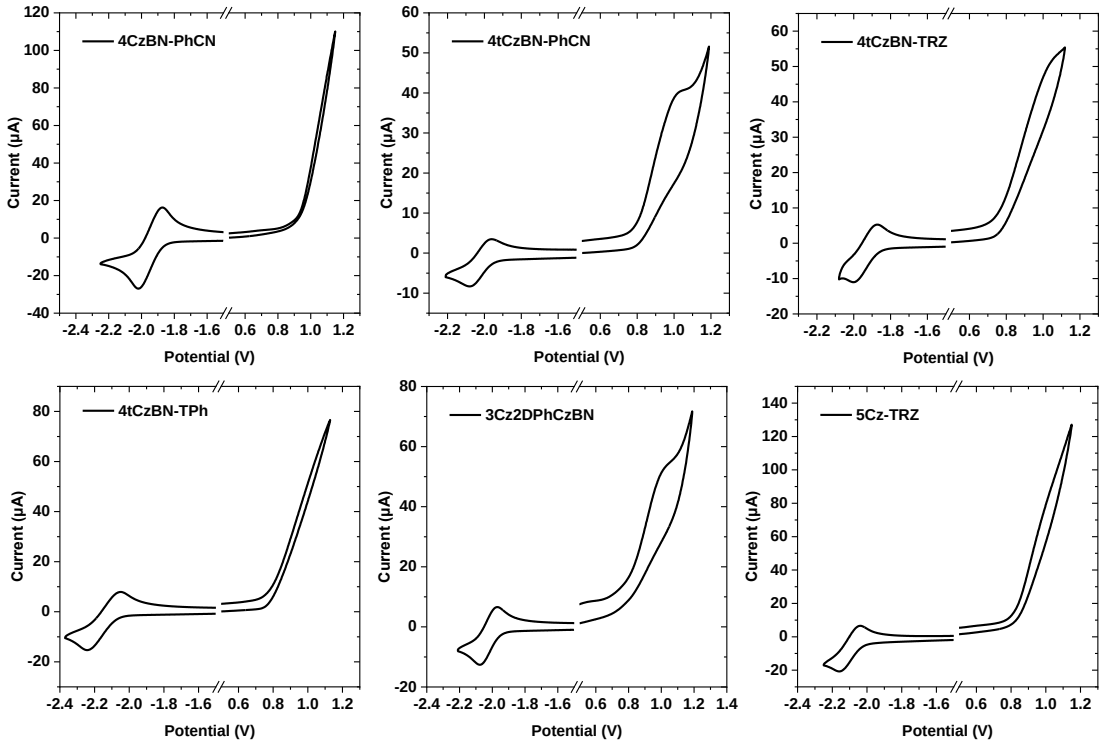

Supplementary Figure 4 CV curves of the TADF emitters

Supplementary Table 4 HOMO, LUMO and E_g of the TADF emitters.

	HOMO [eV]	**LUMO [eV]**	**E_g [eV]**
4CzBN-PhCN	-5.90	-2.81	3.09
4tCzBN-PhCN	-5.68	-2.73	2.95
4tCzBN-TRZ	-5.68	-2.74	2.94
4tCzBN-TPh	-5.71	-2.53	2.98

S4. Photophysical properties

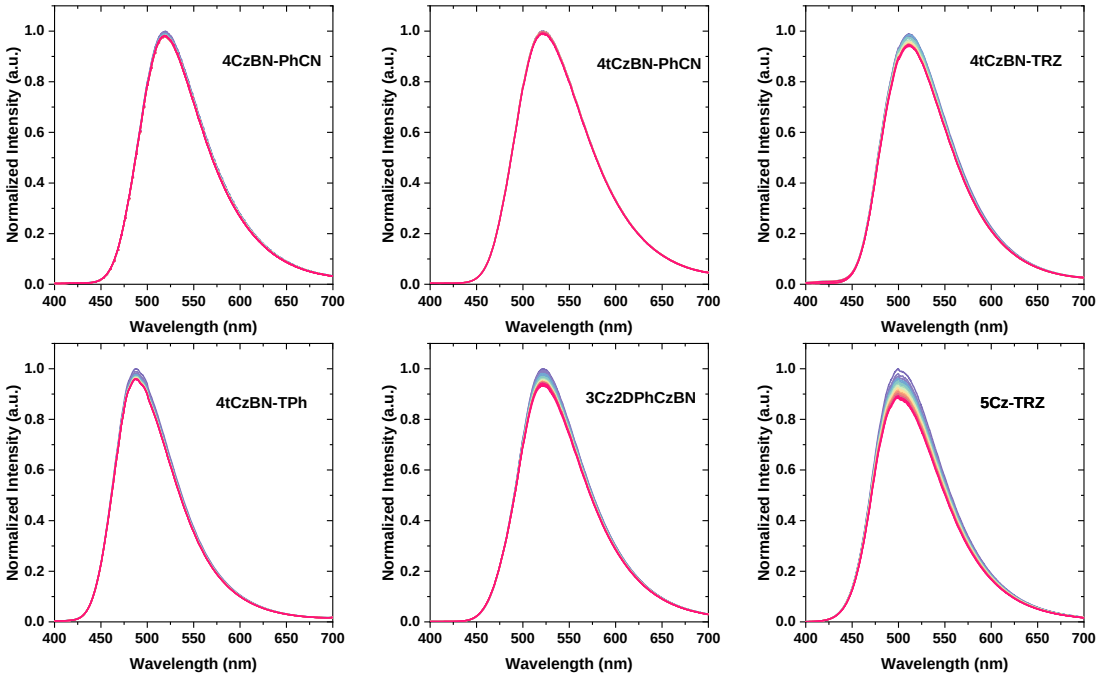

Supplementary Figure 5 Photo-degradation spectra of the TADF-emitters.

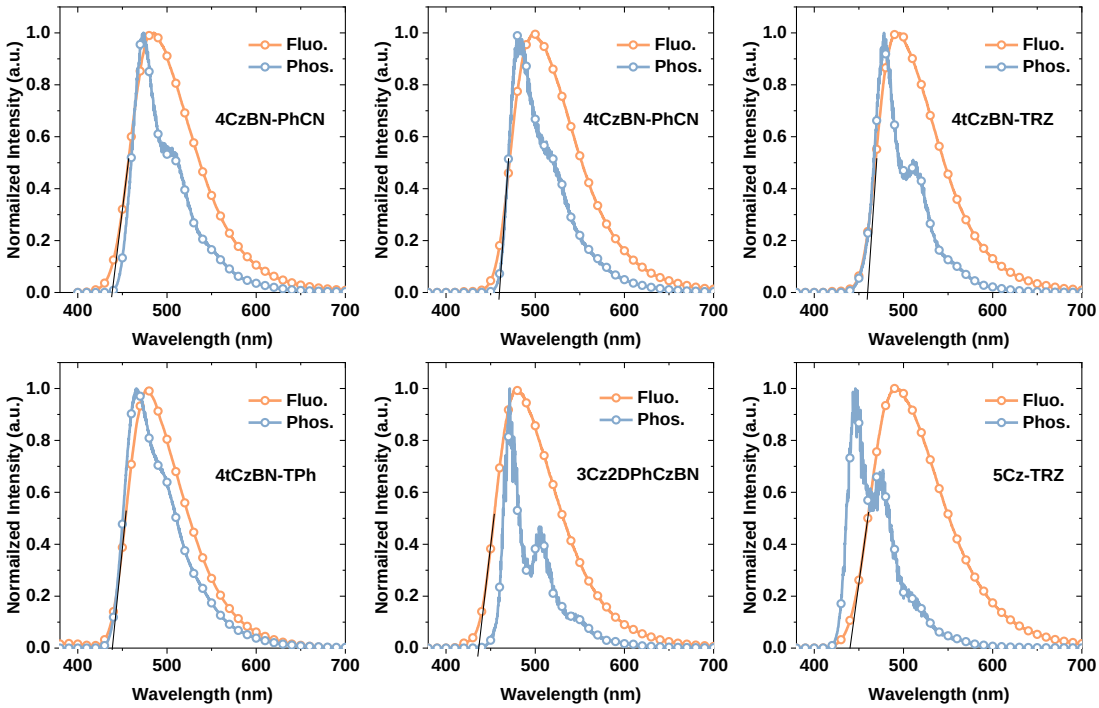

Supplementary Figure 6 Fluorescence and phosphorescence spectra of the TADF-emitters.

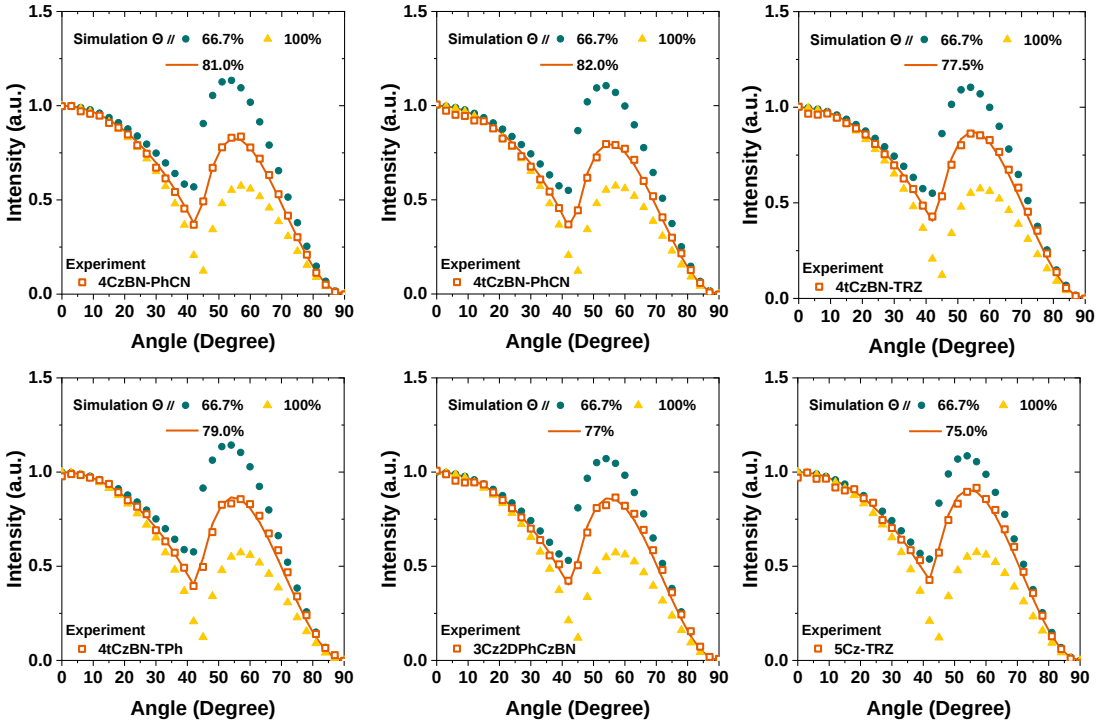

Supplementary Figure 7 Angle-dependent PL spectra of the TADF emitters doped in SiCzCz: SiTrzCz2 films.

S5. Device performance

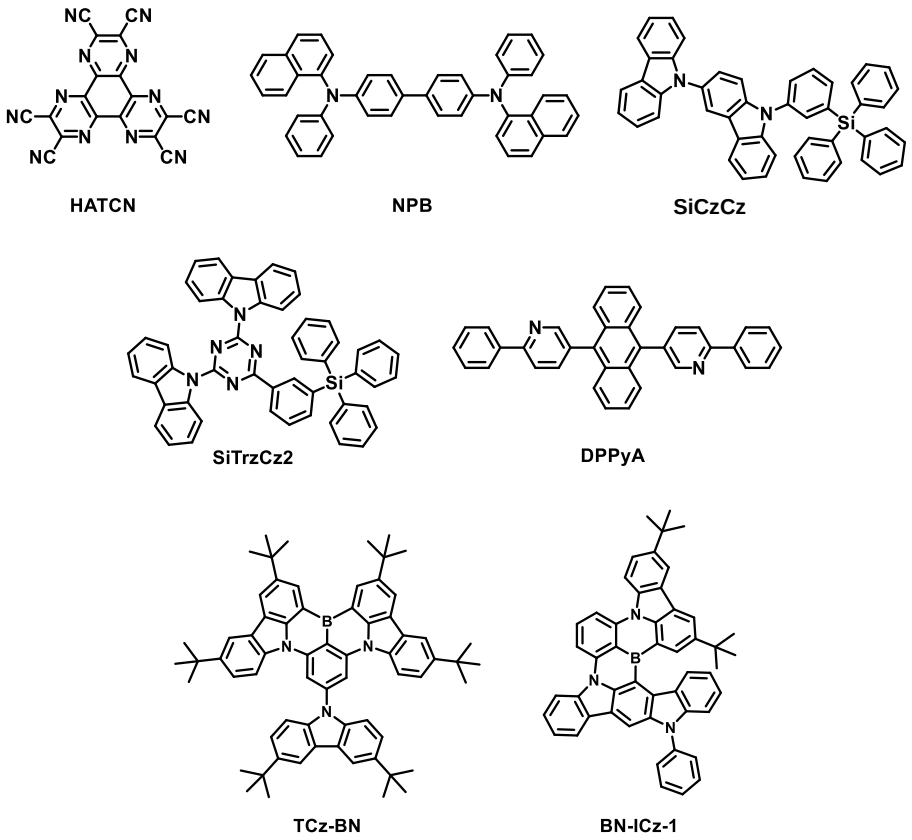

Supplementary Figure 8 The functional materials employed in the devices.

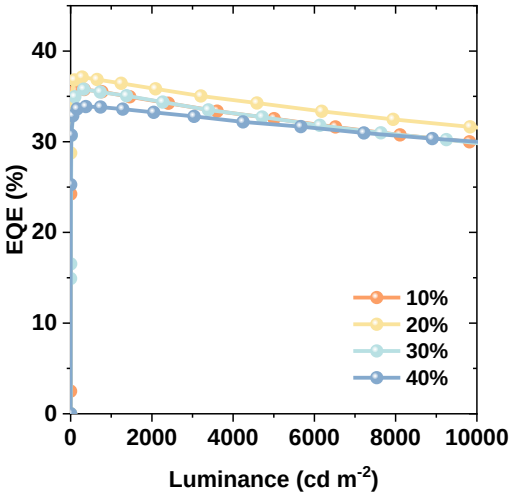

Supplementary Figure 9 EQE-luminance characteristics of 4tCzBN-PhCN devices with different doping concentration.

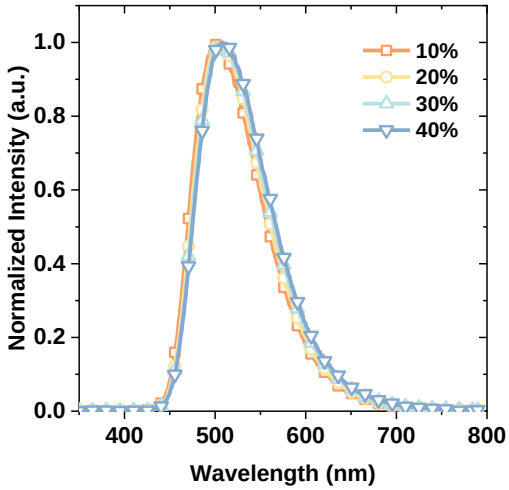

Supplementary Figure 10 EL spectra of 4tCzBN-PhCN devices with different doping concentration.

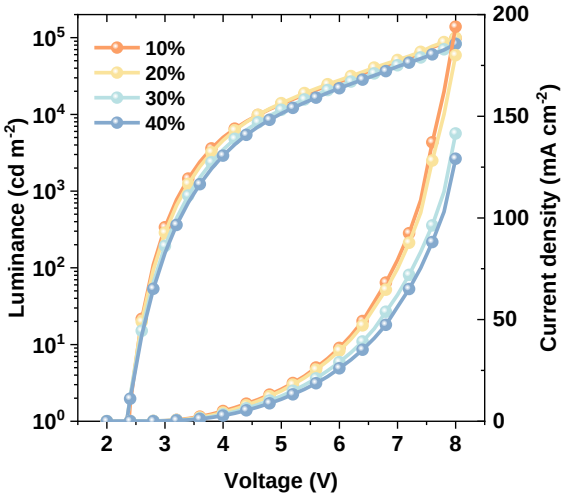

Supplementary Figure 11 J-V-L characteristics of 4tCzBN-PhCN devices with different doping concentration.

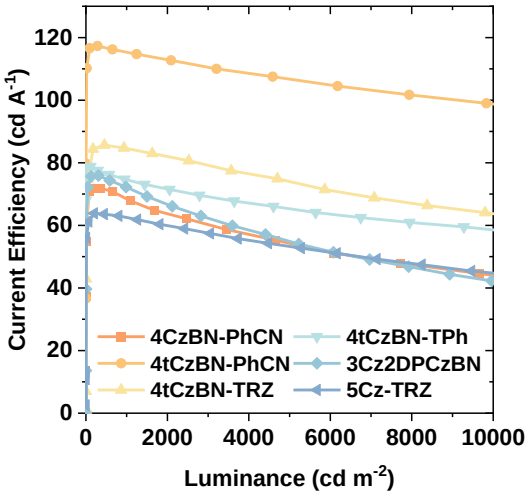

Supplementary Figure 12 Current efficiency-luminance characteristics of the TADF-devices.

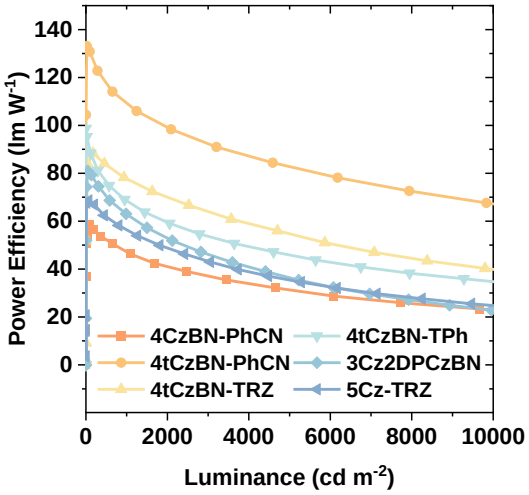

Supplementary Figure 13 Power efficiency-luminance characteristics of the TADF-devices.

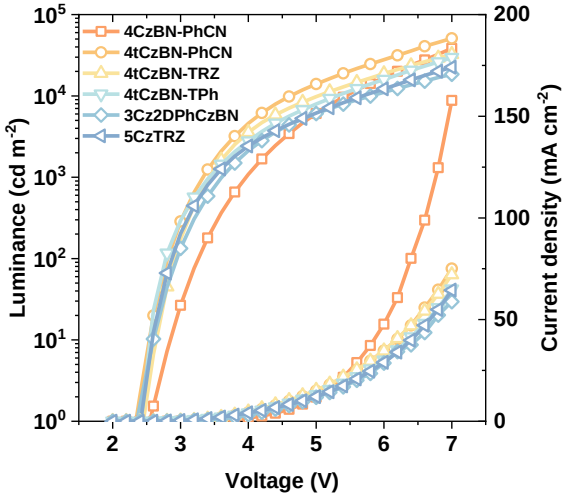

Supplementary Figure 14 J-V-L characteristics of the TADF-devices.

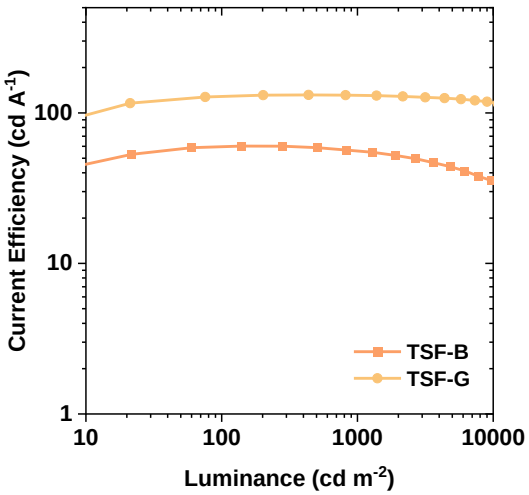

Supplementary Figure 15 Current efficiency-luminance characteristics of the TSF-devices.

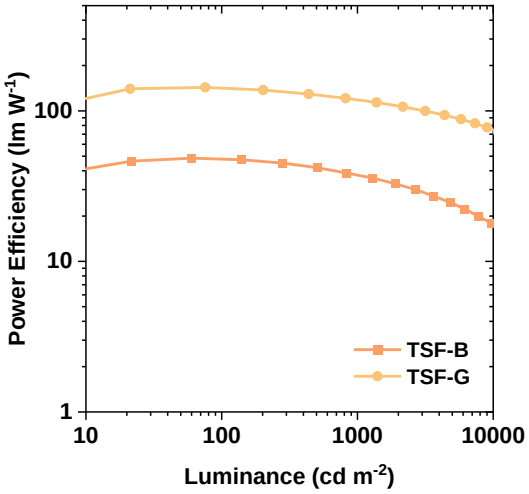

Supplementary Figure 16 Power efficiency-luminance characteristics of the TSF-devices.

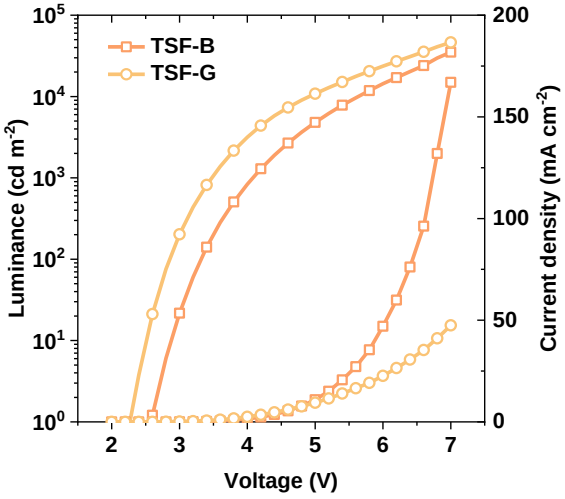

Supplementary Figure 17 J-V-L characteristics of the TSF-devices.

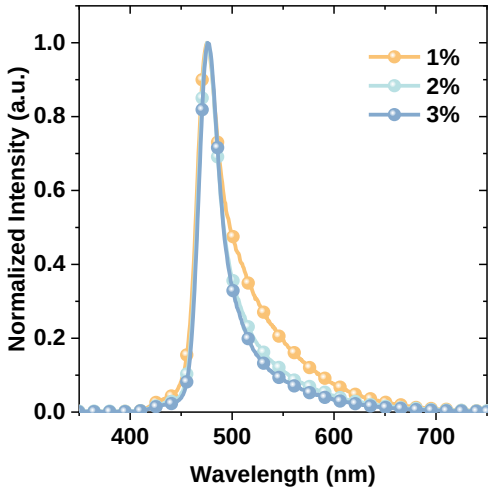

Supplementary Figure 18 EL spectra of TSF-B devices with different MR-emitter doping concentration.

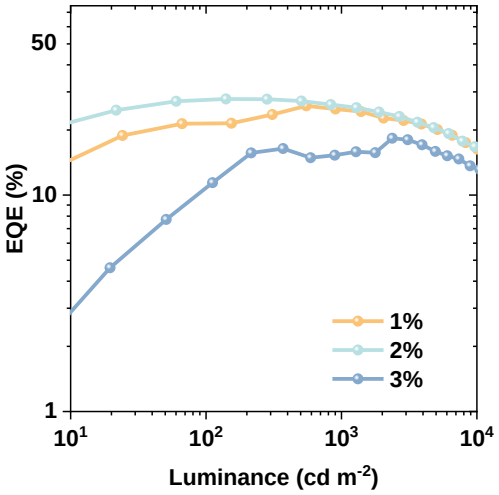

Supplementary Figure 19 EQE-luminance characteristics of TSF-B devices with different MR-emitter doping concentration.

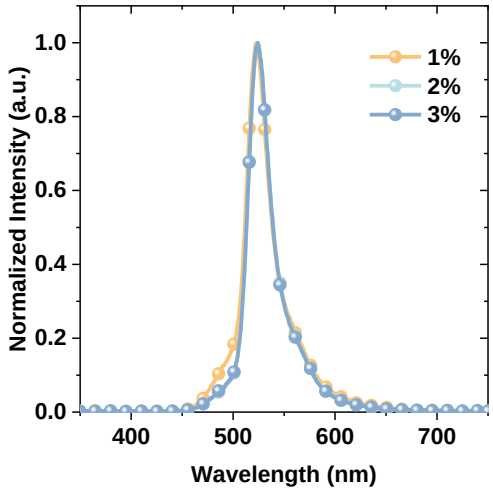

Supplementary Figure 20 EL spectra of TSF-G devices with different MR-emitter doping concentration.

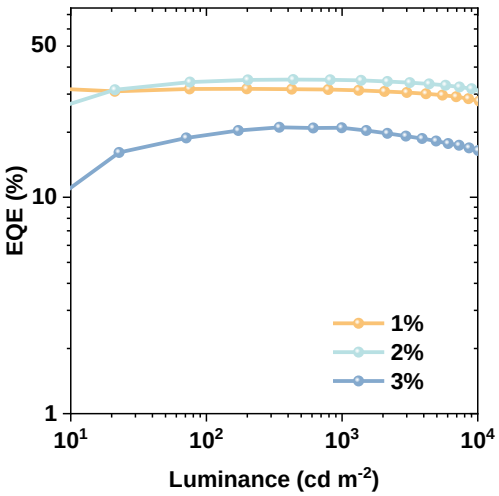

Supplementary Figure 21 EQE-luminance characteristics of TSF-G devices with different MR-emitter doping concentration.

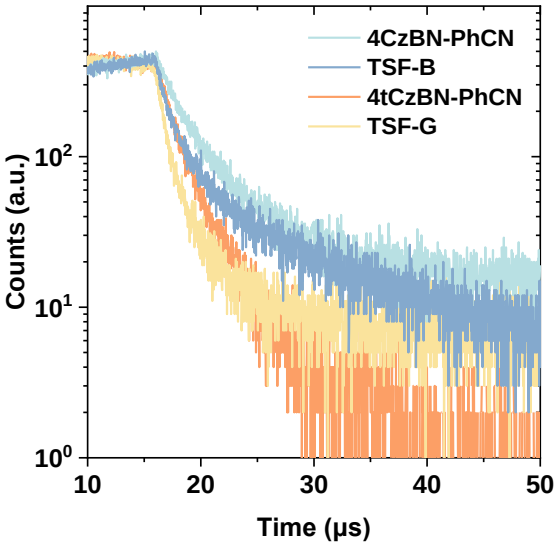

Supplementary Figure 22 Transient electroluminance decay curves of the TADF and TSF-devices.

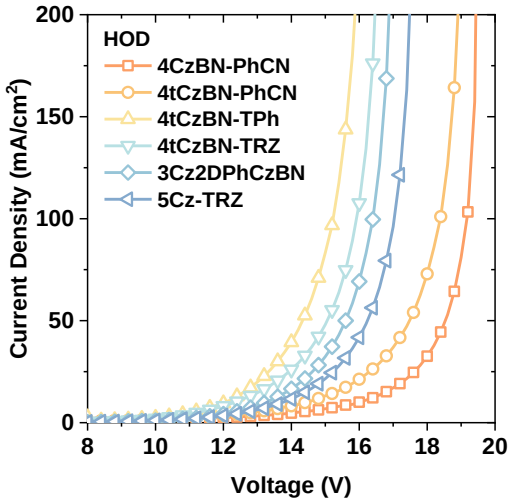

Supplementary Figure 23 J-V-L characteristics of the hole-only devices.

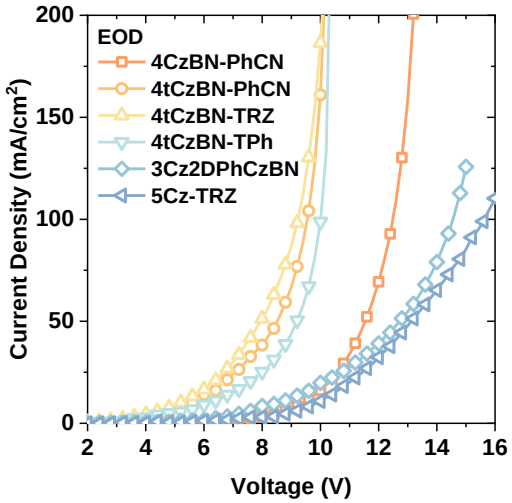

Supplementary Figure 24 J-V-L characteristics of the electron-only devices.

Supplementary Table 5 Summarized CIE_y /LT95 of blue and green TADF/TSF-OLEDs with considerable device operating lifetime.

	LT95 @1000 cd m^{-2} (h)	**CIE_y**	**Ref.**
TSF-B	**460**	**0.27**	**This work**
TSF-G	**2469**	**0.71**	**This work**
p4tCzPhBN	~9	0.12	9
HDT-1 (Tandem)	~20	0.16	8
HDT-1 (Single Emission Layer)	~12	0.2	8
PPCzTrz (Top Emission)	~6	0.17	11
3Ph2CzCzBN	~10	0.36	21
5tCzBN	~20	0.4	7
3Cz2DPhCzBN	~210	0.44	22
ICBNTrz3	~220	0.54	23
4CzIPN	1315	0.58	24
tPhBODIPY	~100	0.66	25

S6. X-ray structural analysis

Supplementary Table 6 X-ray structural information of the TADF materials.

	4CzBN-PhCN	4tCzBN-PhCN	4tCzBN-TRZ	4tCzBN-TPh
CCDC Number	2232729	2232730	2232731	2232732
Empirical formula	$C_{62}H_{36}N_6$	$C_{94}H_{100}N_6$	$2(C_{108}H_{110}N_8)$	$C_{105}H_{109}N_5$
Formula weight	864.97	1313.81	3040.07	1440.97
Crystal system	Monoclinic	Triclinic	Triclinic	Monoclinic
***T* (K)**	170	173	293	293
space group	P21/c	P-1	P-1	I2/a
***a*/Å**	12.3683(2)	11.3892(4)	17.5848(4)	22.3924(3)
***b*/Å**	9.5383(2)	15.5799(6)	18.0059(4)	20.2088(2)
***c*/Å**	37.6166(12)	23.4822(10)	33.6335(7)	21.9560(2)
***α*/ °**	90	100.858(3)	87.395(2)	90
***β*/ °**	95.220(2)	91.212(3)	84.576(2)	105.202(1)
***γ*/ °**	90	99.560(3)	64.102(2)	90
***V*/Å^3**	4419.32(18)	4029.4(3)	9536.9(4)	9587.93(19)
Z	4	2	2	4
density, g/cm^3	1.300	1.083	1.059	0.998
F (000)	1800	1412.0	3256.0	3096.0
h,k,l$_{max}$	14,10,42	14,19,29	22,22,42	25,22,24
N$_{ref}$	6708	16004	38047	7358
μ (mm^{-1})	0.601	0.474	0.468	0.433
***R1* (all data)**	0.0727(5521)	0.0590(13055)	0.0850(29423)	0.0427(6528)
***wR2* (all data)**	0.2122(6708)	0.1765(16004)	0.2642(38047)	0.1196(7358)

S7. NMR and MALDI-TOF-MS spectra

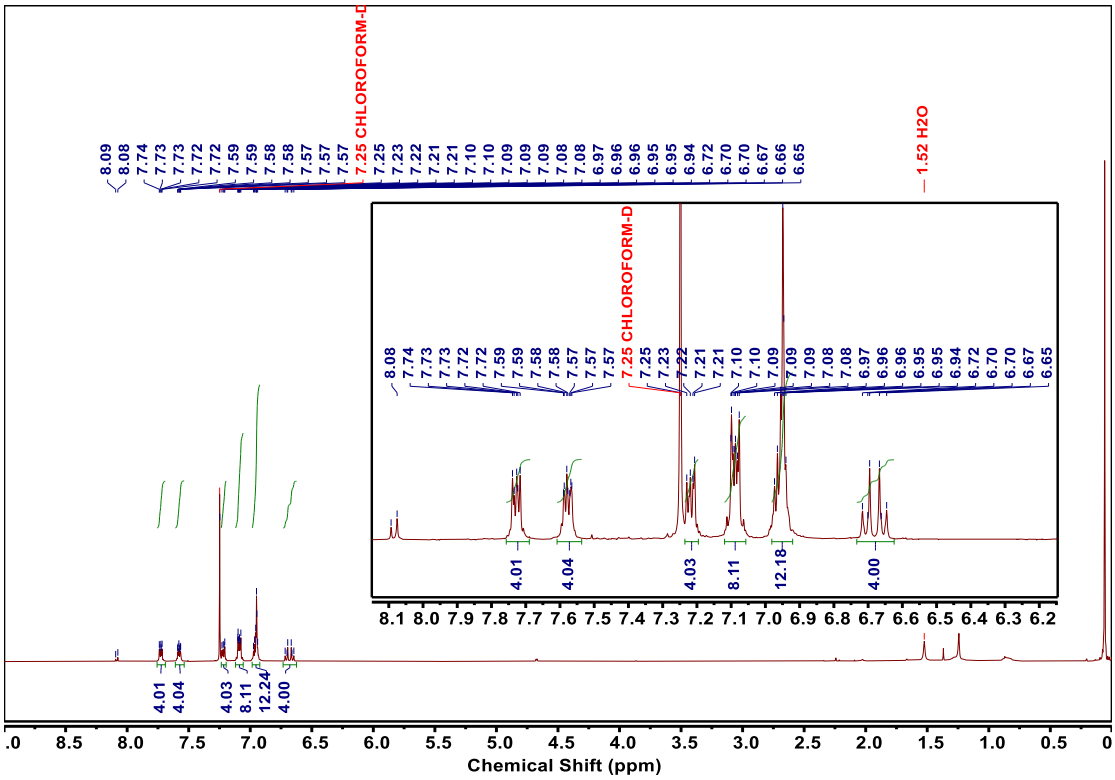

Supplementary Figure 25 ^{1}H NMR of 4CzBN-PhCN

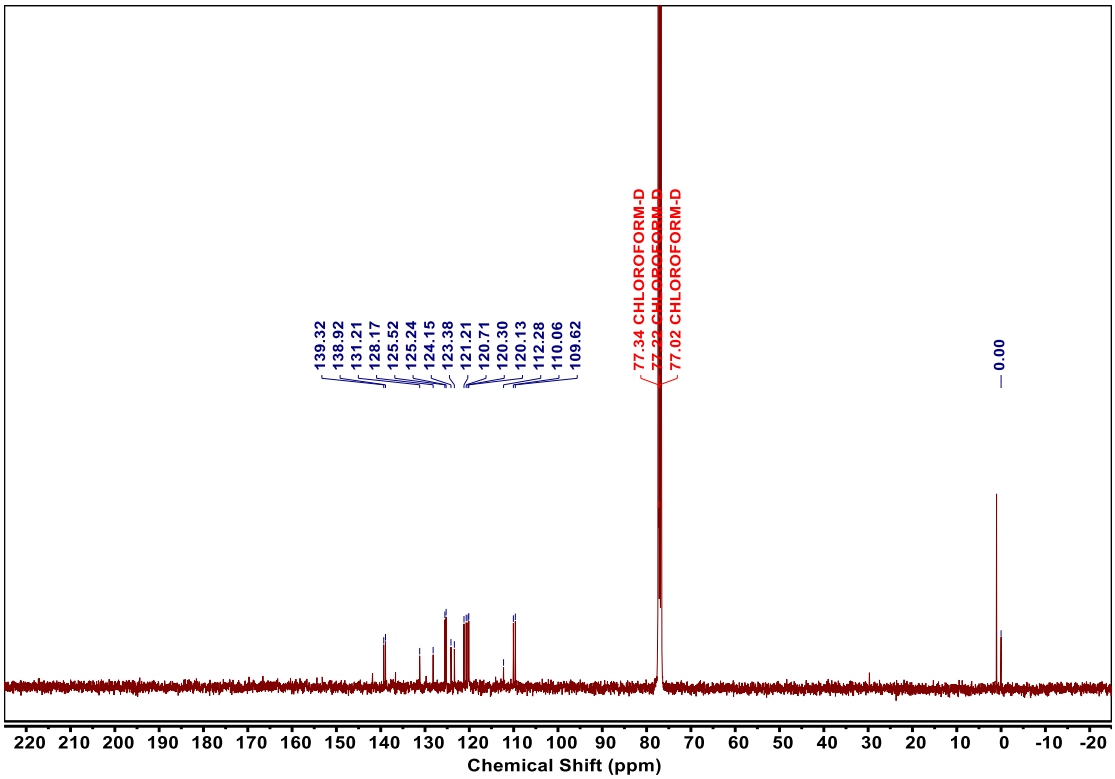

Supplementary Figure 26 ^{13}C NMR of 4CzBN-PhCN

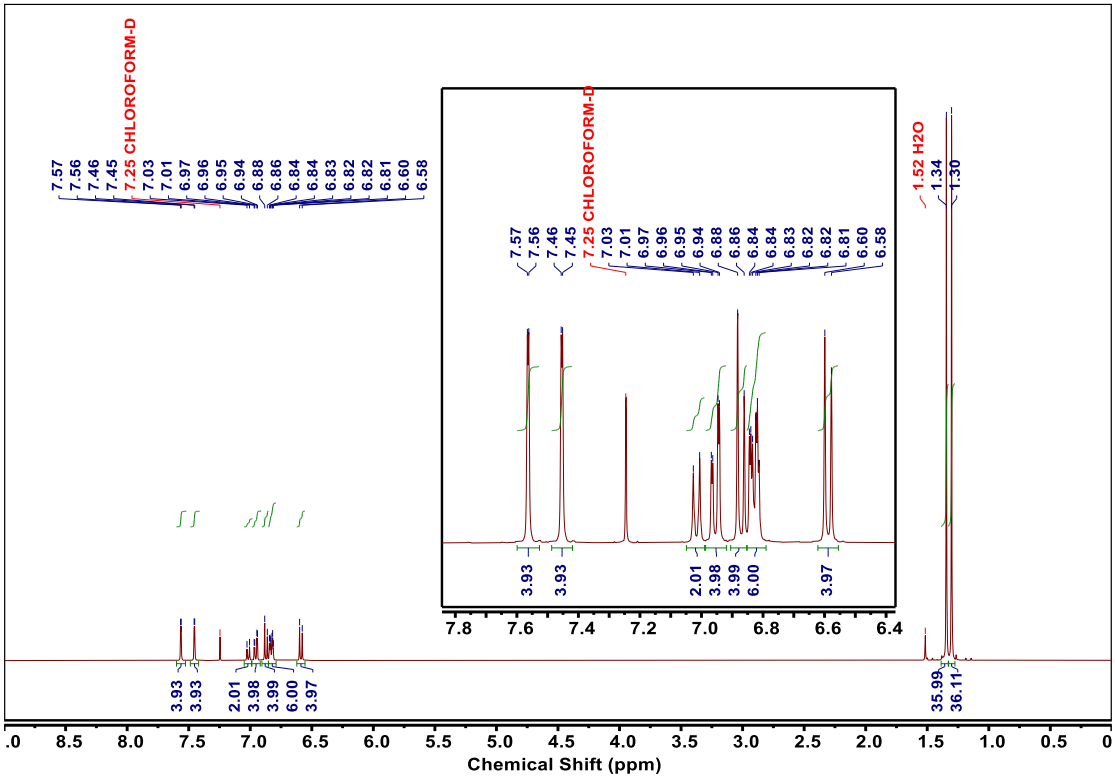

Supplementary Figure 27 ^{1}H NMR of 4tCzBN-PhCN

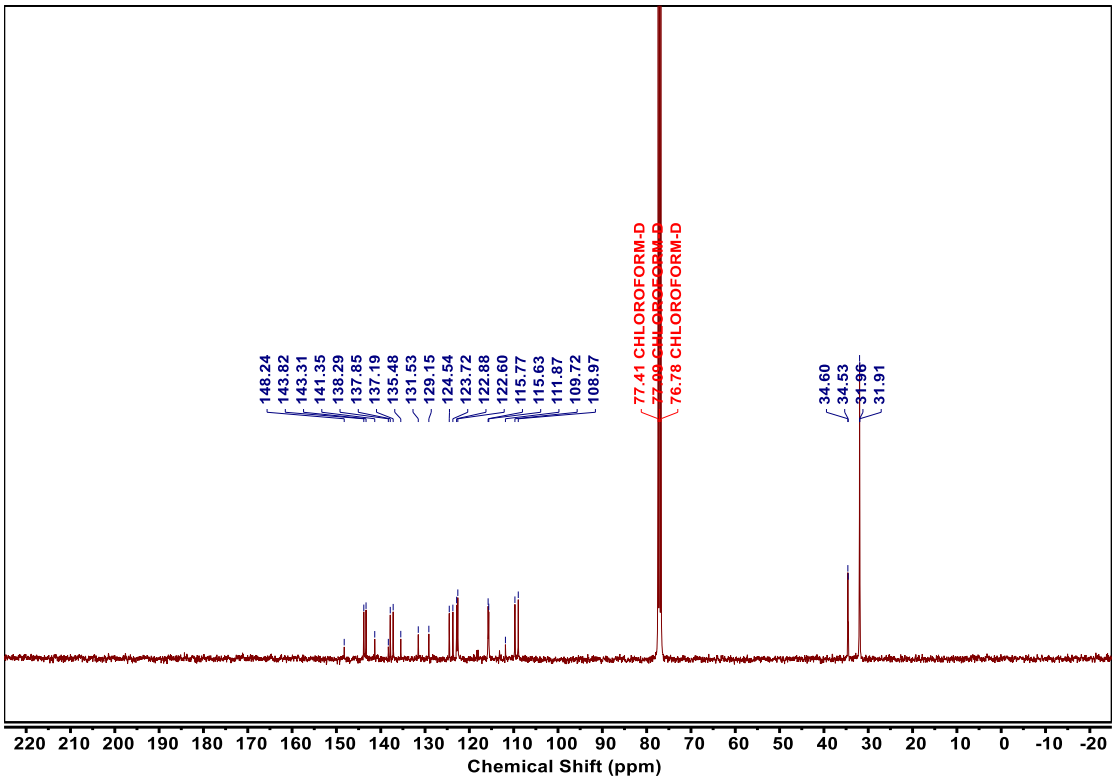

Supplementary Figure 28 ^{13}C NMR of 4tCzBN-PhCN

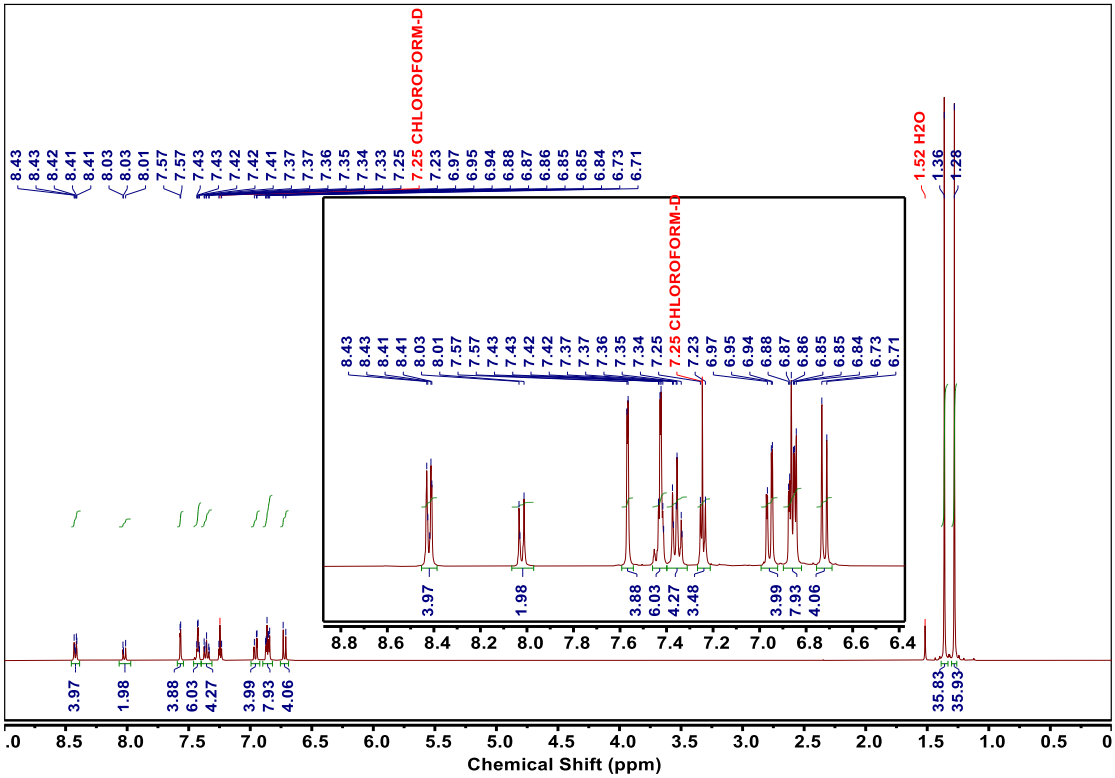

Supplementary Figure 29 ^{1}H NMR of 4tCzBN-TRZ

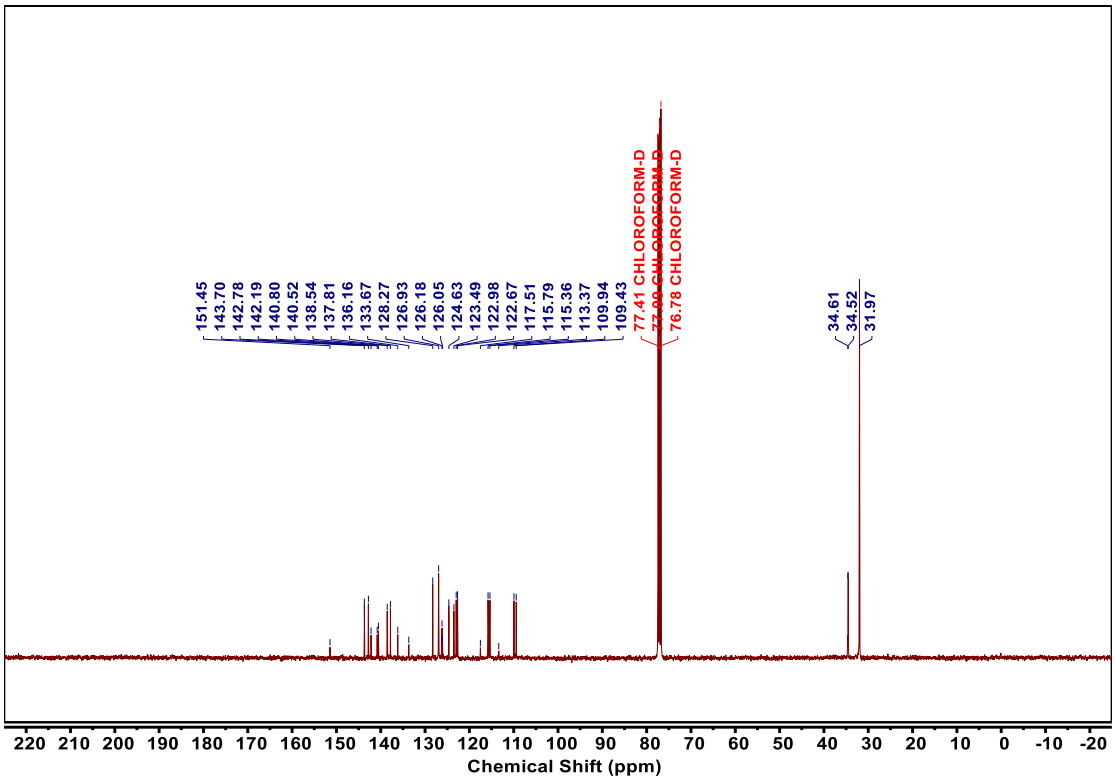

Supplementary Figure 30 ^{13}C NMR of 4tCzBN-TRZ

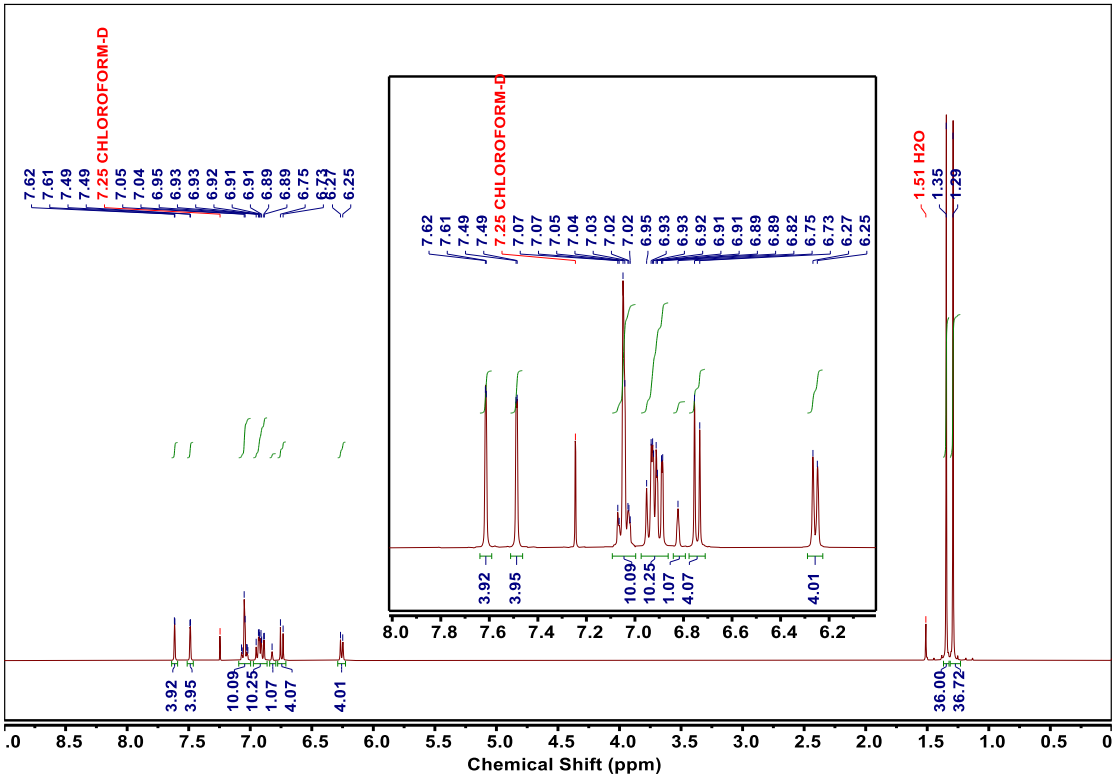

Supplementary Figure 31 ^{1}H NMR of 4tCzBN-TPh

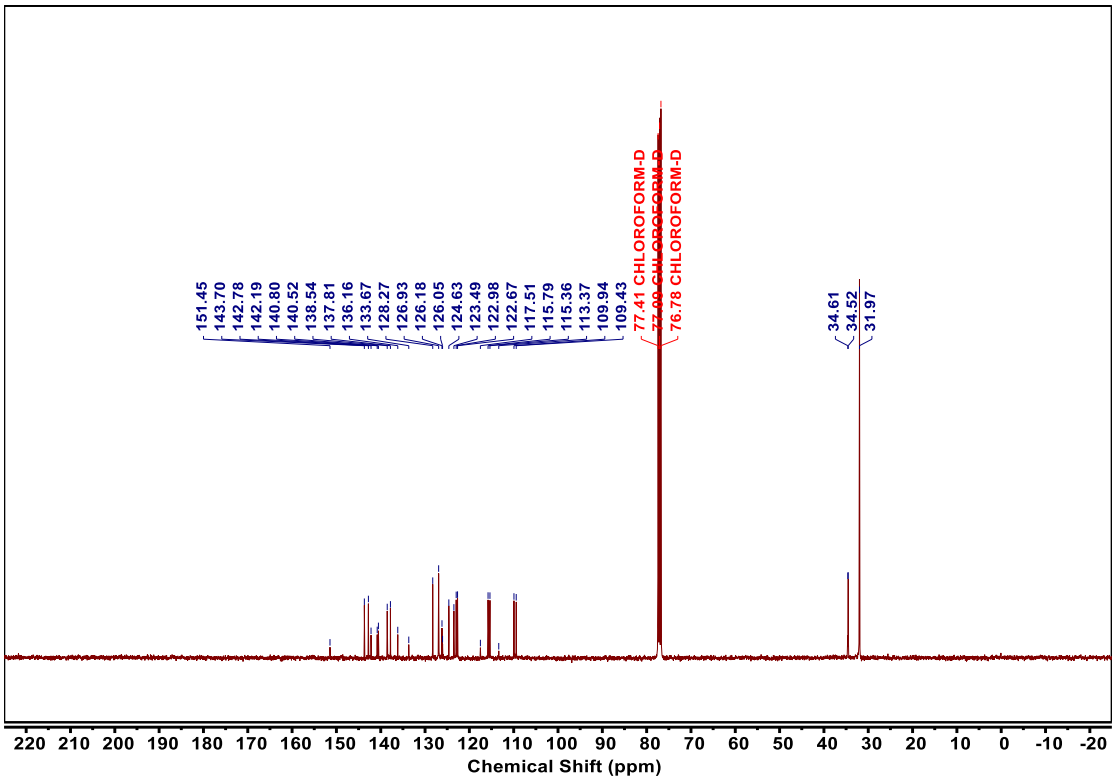

Supplementary Figure 32 ^{13}C NMR of 4tCzBN-TPh

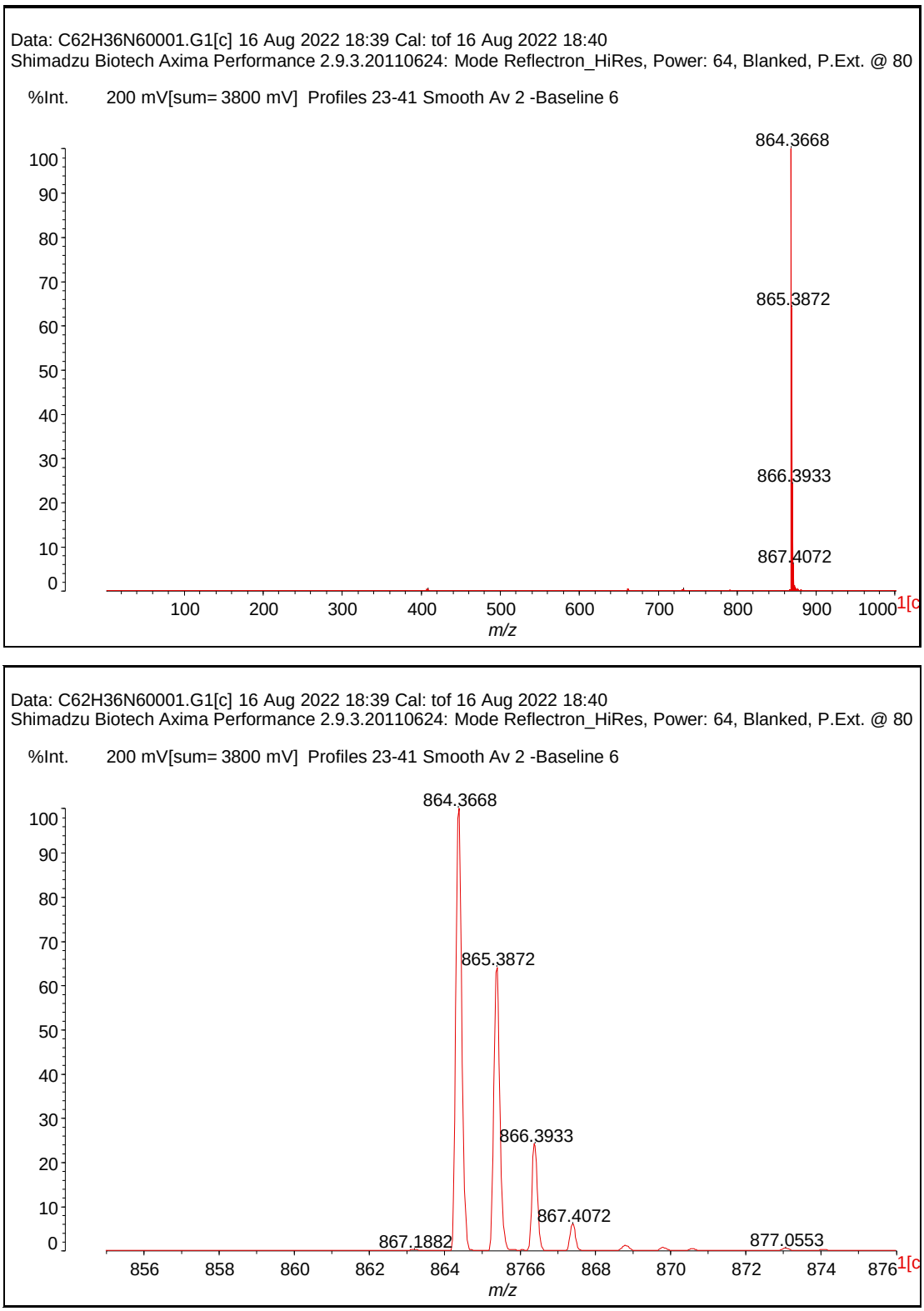

Supplementary Figure 33 MALDI-TOF-MS of 4CzBN-PhCN

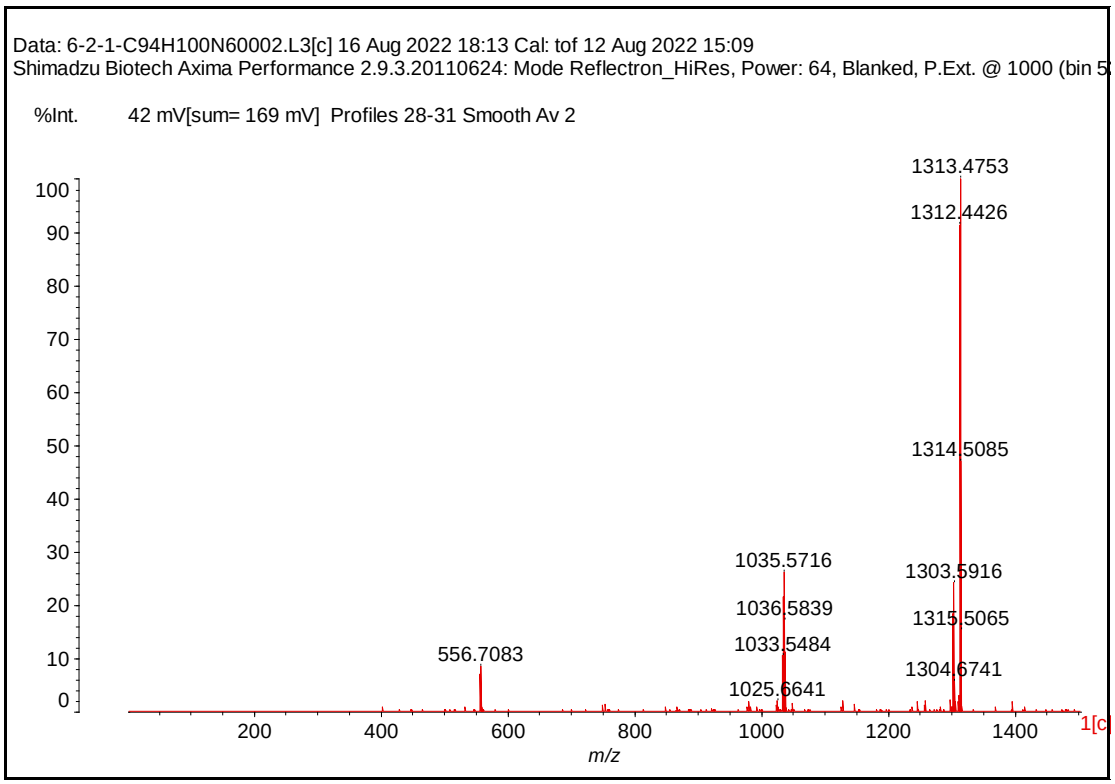

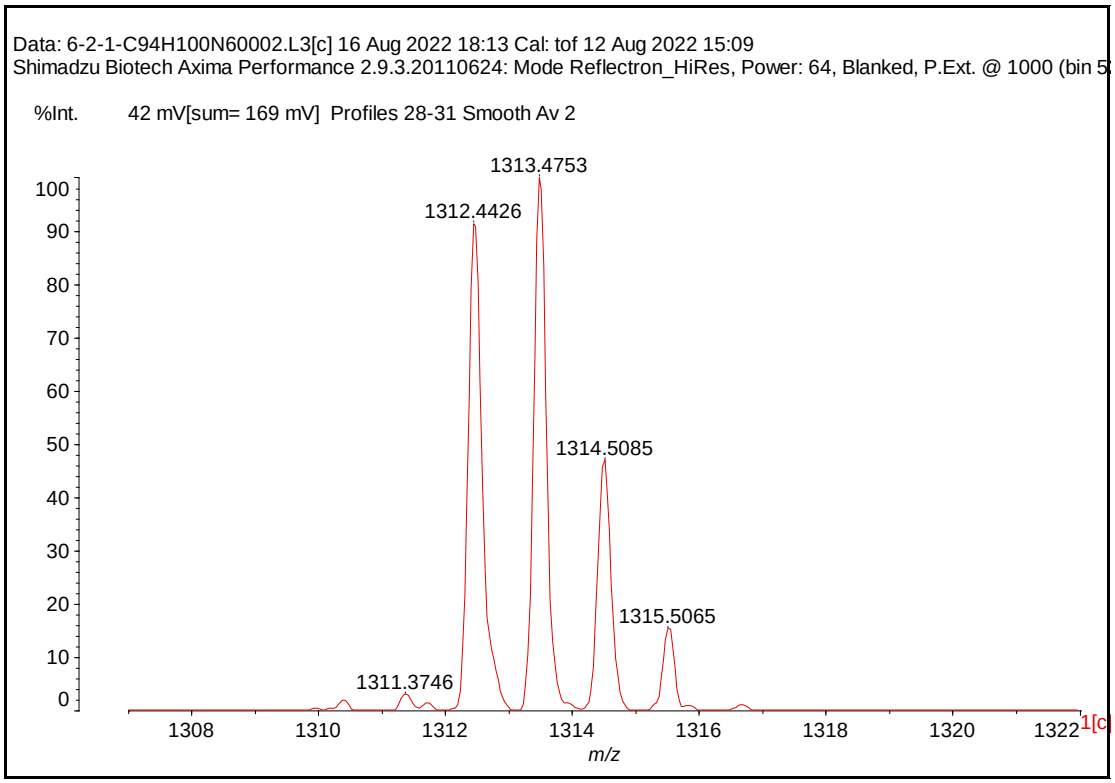

Supplementary Figure 34 MALDI-TOF-MS of 4tCzBN-PhCN

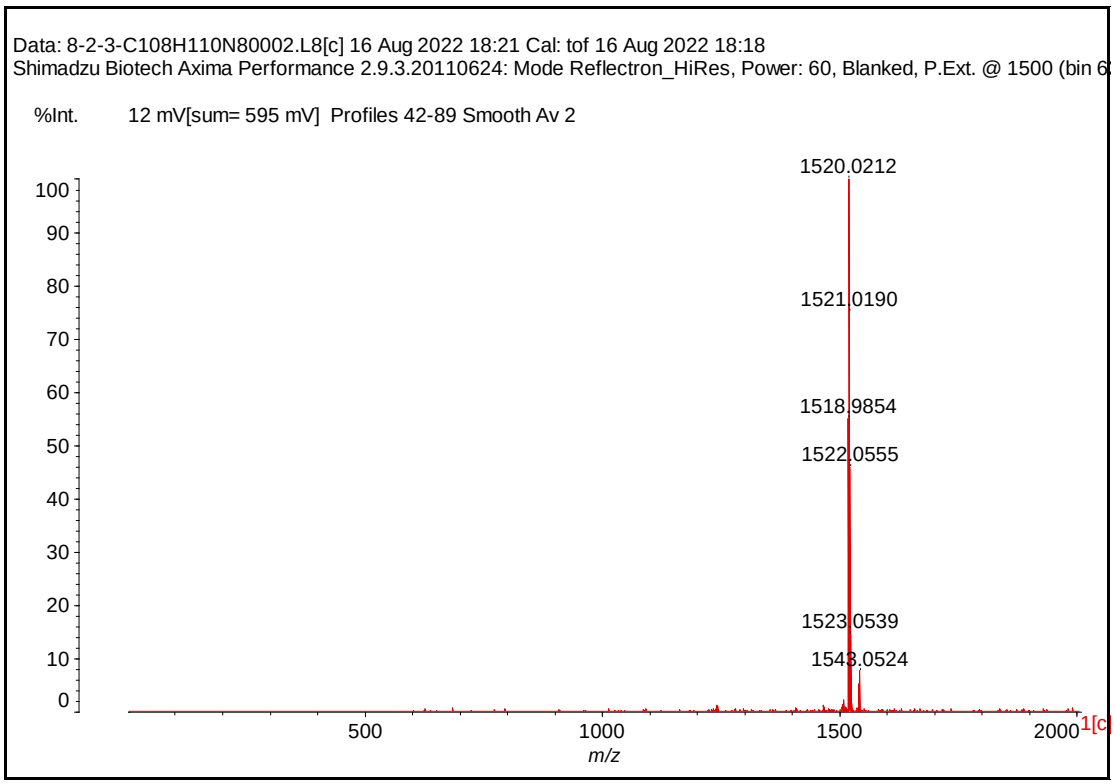

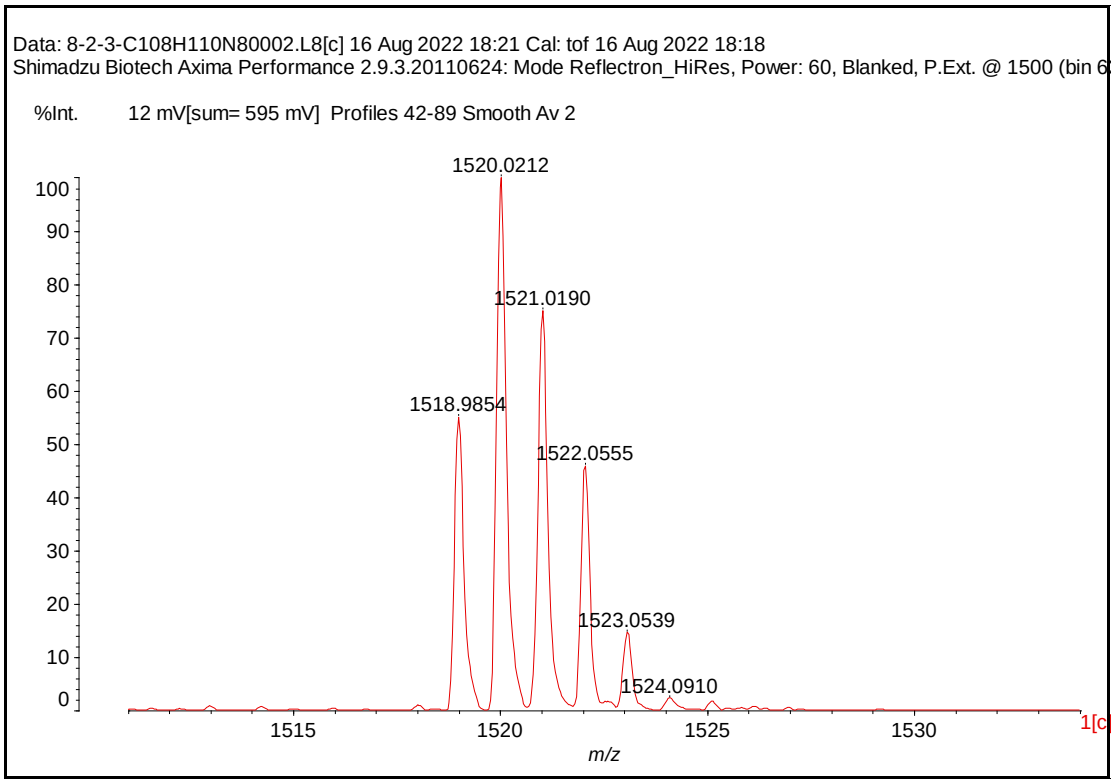

Supplementary Figure 35 MALDI-TOF-MS of 4tCzBN-TRZ

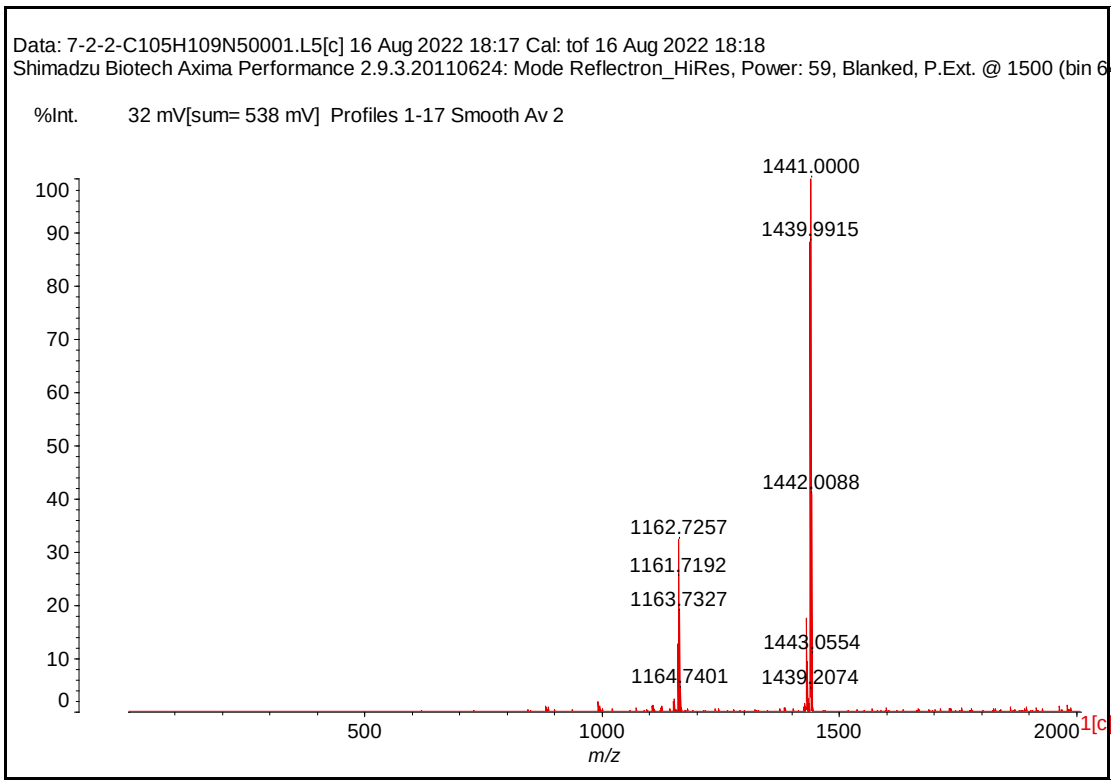

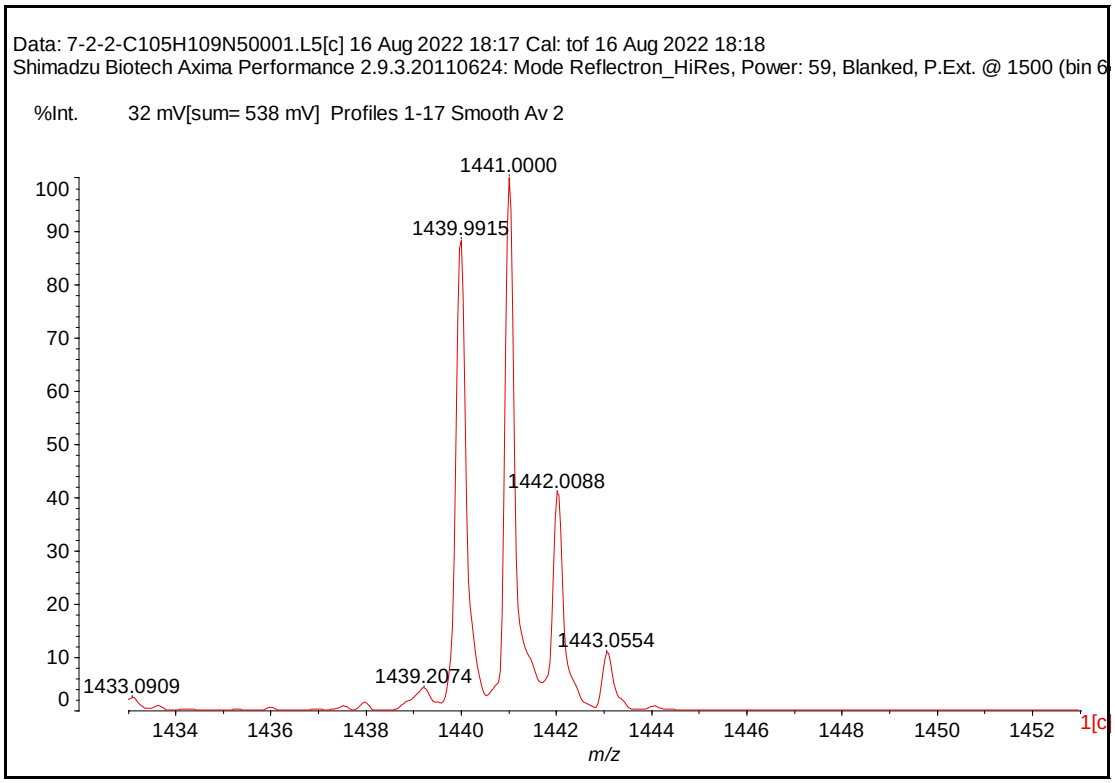

Supplementary Figure 36 MALDI-TOF-MS of 4tCzBN-TPh

S8. References

1. Frisch, M. J. *et al.* Gaussian 16 Revision B.01. (2016).
2. Neese, F. The ORCA program system. *WIREs Comput Mol Sci* **2**, 73–78 (2012).
3. Lu, T. & Chen, F. Multiwfn: A multifunctional wavefunction analyzer. *J. Comput. Chem.* **33**, 580–592 (2012).
4. Liu, Z., Lu, T. & Chen, Q. An sp-hybridized all-carboatomic ring, cyclo[18]carbon: Electronic structure, electronic spectrum, and optical nonlinearity. *Carbon* **165**, 461–467 (2020).
5. Masui, K., Nakanotani, H. & Adachi, C. Analysis of exciton annihilation in high-efficiency sky-blue organic light-emitting diodes with thermally activated delayed fluorescence. *Org. Electron.* **14**, 2721–2726 (2013).
6. Uoyama, H., Goushi, K., Shizu, K., Nomura, H. & Adachi, C. Highly efficient organic light-emitting diodes from delayed fluorescence. *Nature* **492**, 234–238 (2012).
7. Zhang, D., Cai, M., Zhang, Y., Zhang, D. & Duan, L. Sterically shielded blue thermally activated delayed fluorescence emitters with improved efficiency and stability. *Mater. Horiz.* **3**, 145–151 (2016).
8. Chan, C.-Y. *et al.* Stable pure-blue hyperfluorescence organic light-emitting diodes with high-efficiency and narrow emission. *Nat. Photonics* **15**, 203–207 (2021).
9. Zhang, D. *et al.* Efficient and Stable Deep-Blue Fluorescent Organic Light-Emitting Diodes Employing a Sensitizer with Fast Triplet Upconversion. *Adv. Mater.* **32**, 1908355 (2020).
10. Kaji, H. *et al.* Purely organic electroluminescent material realizing 100% conversion from electricity to light. *Nat Commun* **6**, 8476 (2015).
11. Jeon, S. O. *et al.* High-efficiency, long-lifetime deep-blue organic light-emitting diodes. *Nat. Photonics* **15**, 208–215 (2021).
12. Hong, X. *et al.* TADF molecules with π-extended acceptors for simplified high-efficiency blue and white organic light-emitting diodes. *Chem* **8**, 1705–1719 (2022).
13. Wada, Y., Nakagawa, H., Matsumoto, S., Wakisaka, Y. & Kaji, H. Organic light emitters exhibiting very fast reverse intersystem crossing. *Nat. Photonics* **14**, 643–649 (2020).
14. Ahn, D. H. *et al.* Highly efficient blue thermally activated delayed fluorescence emitters based on symmetrical and rigid oxygen-bridged boron acceptors. *Nat. Photonics* **13**, 540–546 (2019).
15. Chen, Y. *et al.* Approaching Nearly 40% External Quantum Efficiency in Organic Light Emitting Diodes Utilizing a Green Thermally Activated Delayed Fluorescence Emitter with an Extended Linear Donor–Acceptor–Donor Structure. *Adv. Mater.* 2103293 (2021).
16. Kim, J. U. *et al.* Nanosecond-time-scale delayed fluorescence molecule for deep-blue OLEDs with small efficiency rolloff. *Nat Commun* **11**, 1765 (2020).
17. Tanaka, H., Shizu, K., Miyazaki, H. & Adachi, C. Efficient green thermally activated delayed fluorescence (TADF) from a phenoxazine–triphenyltriazine (PXZ–TRZ) derivative. *Chem. Commun.* **48**, 11392 (2012).
18. Zeng, W. *et al.* Achieving Nearly 30% External Quantum Efficiency for Orange-Red Organic Light Emitting Diodes by Employing Thermally Activated Delayed Fluorescence Emitters Composed of 1,8-Naphthalimide-Acridine Hybrids. *Adv. Mater.* **30**, 1704961 (2018).
19. Wu, T.-L. *et al.* Diboron compound-based organic light-emitting diodes with high efficiency and reduced efficiency roll-off. *Nature Photon* **12**, 235–240 (2018).
20. Hirata, S. *et al.* Highly efficient blue electroluminescence based on thermally activated delayed fluorescence. *Nat. Mater.* **14**, 330–336 (2015).

21. Chan, C.-Y., Tanaka, M., Nakanotani, H. & Adachi, C. Efficient and stable sky-blue delayed fluorescence organic light-emitting diodes with CIEy below 0.4. *Nat. Commun.* **9**, 5036 (2018).
22. Noda, H., Nakanotani, H. & Adachi, C. Excited state engineering for efficient reverse intersystem crossing. *Sci. Adv.* **4**, eaao6910 (2018).
23. Lee, H. J., Lee, H. L., Han, S. H. & Lee, J. Y. Novel secondary acceptor based molecular design for superb lifetime in thermally activated delayed fluorescent organic light-emitting diodes through high bond energy and fast up-conversion. *Chemical Engineering Journal* **427**, 130988 (2022).
24. Tsang, D. P.-K., Matsushima, T. & Adachi, C. Operational stability enhancement in organic light-emitting diodes with ultrathin Liq interlayers. *Sci Rep* **6**, 22463 (2016).
25. Song, X., Zhang, D., Zhang, Y., Lu, Y. & Duan, L. Strategically Modulating Carriers and Excitons for Efficient and Stable Ultrapure-Green Fluorescent OLEDs with a Sterically Hindered BODIPY Dopant. *Adv. Optical Mater.* **8**, 2000483 (2020).